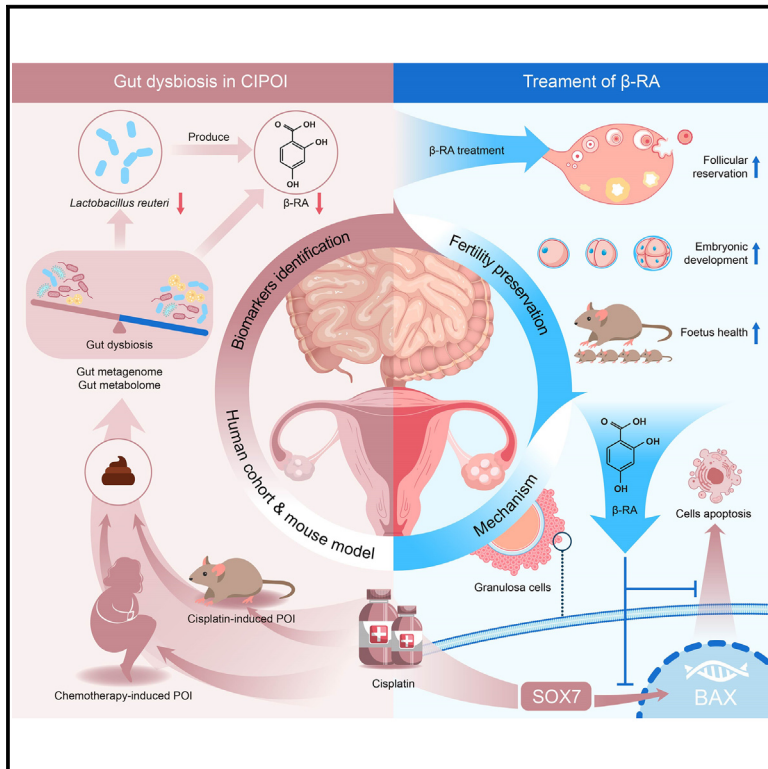


# $\beta$ -resorcylic acid released by *Limosilactobacillus reuteri* protects against cisplatin-induced ovarian toxicity and infertility

## Graphical abstract



## Authors

Yinglin Feng, Huimin Zheng, Chunhua Yin, ..., Guoqiang Chen, Pan Li, Xia Chen

## Correspondence

cxq2316@163.com (X.C.),  
13929981788@139.com (G.C.),  
pan.li@unsw.edu.au (P.L.),  
chenx\_fsyyy@163.com (X.C.)

## In brief

Subfertility is a significant adverse effect of chemotherapy in reproductive-age females. Feng et al. identify that *Limosilactobacillus reuteri* and its catabolite,  $\beta$ -resorcylic acid, protect against chemotherapy-induced subfertility by inhibiting granulosa cell apoptosis through the SOX7-BAX axis. These findings suggest promising approaches for preventing chemotherapy-induced subfertility via the “gut-ovary axis.”

## Highlights

- Gut bacteria and metabolite patterns are altered in premature ovarian insufficiency patients
- *Limosilactobacillus reuteri* intake protects against chemotherapy-induced subfertility
- $\beta$ -resorcylic acid, a gut bacterial catabolite, also exerts protective effects
- $\beta$ -resorcylic acid inhibits granulosa cell apoptosis via reduction in nuclear SOX7



## Article

 **$\beta$ -resorcylic acid released by *Limosilactobacillus reuteri* protects against cisplatin-induced ovarian toxicity and infertility**

Yinglin Feng,<sup>1,2,3,14</sup> Huimin Zheng,<sup>1,14</sup> Chunhua Yin,<sup>4,14</sup> Dong Liang,<sup>5</sup> Siyou Zhang,<sup>5</sup> Jingrui Chen,<sup>5</sup> Feihong Mai,<sup>6</sup> Zixin Lan,<sup>7</sup> Menglin Zhu,<sup>7</sup> Zhensheng Mai,<sup>5</sup> Sj Shen,<sup>8</sup> Thisun Jayawardana,<sup>8</sup> Rong Wu,<sup>9</sup> Wenli Tang,<sup>1</sup> Renfang Zhang,<sup>4</sup> Xiaoyun He,<sup>4</sup> Shanshan Zheng,<sup>10</sup> Qian Hu,<sup>11</sup> Yubin Han,<sup>5</sup> Yuanhao Yang,<sup>12,13</sup> Shenhai Gong,<sup>9</sup> Zhang Wang,<sup>6</sup> Emad M. El-Omar,<sup>8</sup> Wei Luo,<sup>11</sup> Xueqin Chen,<sup>1,2,\*</sup> Guoqiang Chen,<sup>11,\*</sup> Pan Li,<sup>8,\*</sup> and Xia Chen<sup>1,2,15,\*</sup>

<sup>1</sup>Central Laboratory of the Medical Research Center, The First Affiliated Hospital of Ningbo University, Ningbo, Zhejiang Province, China

<sup>2</sup>Department of Obstetrics and Gynecology, The First Affiliated Hospital of Ningbo University, Ningbo, Zhejiang Province, China

<sup>3</sup>Department of Obstetrics, Affiliated Foshan Maternity & Child Healthcare Hospital, Southern Medical University, Foshan, Guangdong Province, China

<sup>4</sup>Department of Gynecology and Obstetrics, First Affiliated Hospital of Nanchang University, Nanchang, Jiangxi Province, China

<sup>5</sup>Department of Obstetrics and Gynecology, The First People's Hospital of Foshan, Foshan, Guangdong Province, China

<sup>6</sup>Institute of Ecological Science, School of Life Science, South China Normal University, Guangzhou, Guangdong Province, China

<sup>7</sup>The Second Clinical Medical College, Southern Medical University, Guangzhou, Guangdong Province, China

<sup>8</sup>UNSW Microbiome Research Centre, St George and Sutherland Clinical Campuses, UNSW Sydney, Sydney, NSW, Australia

<sup>9</sup>School of Traditional Chinese Medicine, Southern Medical University, Guangzhou, China

<sup>10</sup>Health Medical Center, The First People's Hospital of Foshan, Foshan, Guangdong Province, China

<sup>11</sup>Institute of Translational Medicine, The First People's Hospital of Foshan, Foshan, Guangdong Province, China

<sup>12</sup>Mater Research Institute, The University of Queensland, Woolloongabba, QLD 4102, Australia

<sup>13</sup>Institute for Molecular Bioscience, The University of Queensland, St Lucia, QLD 4072, Australia

<sup>14</sup>These authors contributed equally

<sup>15</sup>Lead contact

\*Correspondence: [cxq2316@163.com](mailto:cxq2316@163.com) (X.C.), [13929981788@139.com](mailto:13929981788@139.com) (G.C.), [pan.li@unsw.edu.au](mailto:pan.li@unsw.edu.au) (P.L.), [chenx\\_fsyyy@163.com](mailto:chenx_fsyyy@163.com) (X.C.)  
<https://doi.org/10.1016/j.xcrm.2024.101678>

## SUMMARY

Chemotherapy-induced premature ovarian insufficiency (CPOI) triggers gonadotoxicity in women undergoing cancer treatment, leading to loss of ovarian reserves and subfertility, with no effective therapies available. In our study, fecal microbiota transplantation in a cisplatin-induced POI mouse model reveals that a dysbiotic gut microbiome negatively impacts ovarian health in CPOI. Multi-omics analyses show a significant decrease in *Limosilactobacillus reuteri* and its catabolite,  $\beta$ -resorcylic acid, in the CPOI group in comparison to healthy controls. Supplementation with *L. reuteri* or  $\beta$ -RA mitigates cisplatin-induced hormonal disruptions, morphological damages, and reductions in follicular reserve. Most importantly,  $\beta$ -RA pre-treatment effectively preserves oocyte function, embryonic development, and fetus health, thereby protecting against chemotherapy-induced subfertility. Our results provide evidence that  $\beta$ -RA suppresses the nuclear accumulation of sex-determining region Y-box 7, which in turn reduces Bcl-2-associated X activation and inhibits granulosa cell apoptosis. These findings highlight the therapeutic potential of targeting the gut-ovary axis for fertility preservation in CPOI.

## INTRODUCTION

Premature ovarian insufficiency (POI) is defined by the loss of ovarian activity before the age of 40 and is characterized by amenorrhea with high levels of gonadotropins (in particular, follicle-stimulating hormone [FSH]) and low levels of estradiol (E2), ultimately leading to infertility. Chemotherapy can often cause POI as the ovarian follicle is extremely sensitive to the gonadotoxic effects<sup>1</sup> and is an issue of growing concern. The increasing incidence of this subset of disease, termed chemotherapy-induced POI (CPOI), parallels the incidence trend of various cancers in adolescents and young adults who are still of reproductive age and

intend to conceive.<sup>2,3</sup> However, current management strategies for preserving and restoring fertility ranging from ovulation induction, hormone regulation medications, and oocyte or embryo preservation, to *in vitro* fertilization,<sup>4</sup> require functional oocytes and reproductive organs, which could be irreversibly damaged after chemotherapy.<sup>5</sup> Thus, post-pubertal girls with an urgent need to commence cancer treatment are faced with involuntary childlessness in addition to the immense financial burden that accompanies fertility preservation treatments.<sup>6</sup> Thus, effective therapeutic strategies and options for improving the quality of life and restoring fertility are urgently needed to prevent or mitigate the devastating effects of chemotherapy-induced gonadotoxicity.



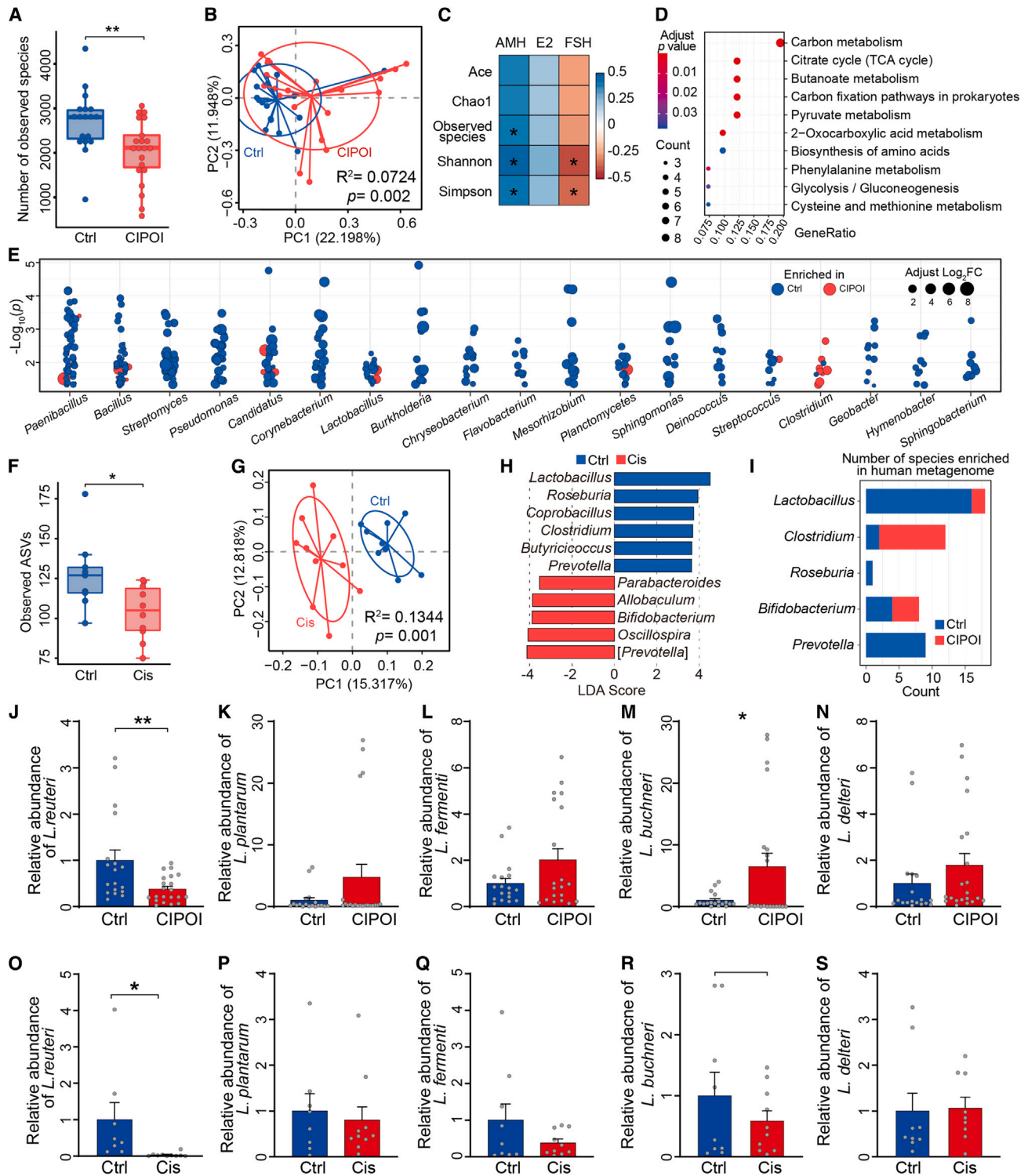


**Figure 1. Dysbiosis of gut microbiota is associated with POI**

(A) Comparison of the number of observed species between CIPOI and control (Ctrl) groups. \*\* $p < 0.01$  by Wilcoxon rank-sum test.

(B) Principal coordinate analysis (PCoA) based on Bray-Curtis distances revealed that the Ctrl bacterial communities clustered separately from CIPOI bacterial communities. Each point represents a single sample, colored by group. Differences in beta diversity between CIPOI and Ctrl were tested by permutational multivariate analysis of variance (PERMANOVA).

(legend continued on next page)

Gut microbiota has an important role in chemotherapy as it regulates both the antitumor effect and toxicity of chemotherapeutic agents.<sup>7,8</sup> Since two milestone studies published in *Science* demonstrated the essential role of gut microbiota in chemotherapy one decade ago,<sup>9,10</sup> emerging evidence suggests the beneficial effect of gut microbiota, as well as the microbial-derived metabolites, in both improving the efficacy of chemotherapy and overcoming chemotherapy-induced side effects.<sup>8,11–13</sup> Moreover, a number of studies have observed alterations of the gut microbiota in patients with ovarian conditions<sup>14,15</sup> and have highlighted the potential of gut microbiota and microbial-derived metabolites in ovary preservation.<sup>16,17</sup> These studies suggested the potential for gut bacteria or bacteria-derived molecules in protecting against damage caused by CIPOI. Although the relationship between gut microbiota and the reproductive system is widely reported,<sup>16,18</sup> the ability of gut bacteria and bacteria-derived metabolites to mitigate gonadotoxicity and infertility is yet to be elucidated.

Cisplatin-based chemotherapy has been clinically proven and is used as the first-line treatment in multiple types of cancers.<sup>19</sup> However, being a cytotoxic drug, cisplatin causes undesirable side effects in different systems, including the reproductive system.<sup>20</sup> There remains a knowledge gap regarding the prevention or reversion of this effect that must be addressed. In the present study, we identified gut bacterial biomarkers from both patients with POI after receiving cisplatin-based combination therapy and a mouse model of cisplatin-induced POI (Cis-POI). Following this, the capability and the related mechanisms of both the bacterium and metabolite in restoring ovarian function and fertility were examined. Collectively, our findings provide promising approaches that target gut microbiota to mitigate Cis-POI and its consequential infertility.

## RESULTS

### Dysbiosis of gut microbiota is associated with CIPOI

For our study, 21 patients who received cisplatin-based combination therapy and developed CIPOI, along with 18 healthy controls, were recruited. We first sought to examine alterations in the gut microbiota by employing whole-genome shotgun sequencing. Patients with CIPOI showed a significant decrease in the number

of bacteria as well as differences in their relative abundance when compared with the control group (Figures 1A, S1A, and S1B) and, additionally, formed a distinct clustering pattern separate from healthy controls (Figure 1B). Bacterial diversity indices were positively correlated with anti-Müllerian hormone (AMH) and negatively correlated with FSH, indicating that lower bacterial diversity might play a role in the development of follicles (Figure 1C). Furthermore, over-representation analysis (ORA) showed that enriched pathways were correlated with energy expenditure and amino acid metabolism (Figure 1D). Thus, we next investigated whether this was due to differences in the taxonomic profiles between patients with CIPOI and healthy controls. We identified 1,582 species belonging to 763 genera (two-sided Wilcoxon rank-sum test,  $p < 0.05$ ; Table S1), of which 19 comprised 10 or more species (Figure 1E). Specifically, most species of *Clostridium* were enriched in patients with CIPOI, whereas most species of the other 18 identified genera, including *Lactobacillus*, *Bacillus*, and *Streptomyces*, were enriched in healthy controls.

Subsequently, to examine whether gut dysbiosis also exists in an experimental setting, we utilized a well-established mouse model of Cis-POI (Figure S1C). Mice with Cis-POI exhibited significant reductions in the weight of ovaries and the number of primordial and antral follicles when compared to control mice, indicating damage to ovary morphology and ovarian reserve reduction. In addition, mice with Cis-POI showed lower serum concentrations of E2 and higher serum concentrations of FSH (Figures S1D–S1G), signifying marked disruptions to sex hormone levels. As evidenced by transmission electron microscopy and TUNEL assay, the disordered arrangement of granulosa cells and the higher apoptotic index were observed in Cis-POI mice (Figures S1H and S1I). Together, these changes in ovarian damage and sex hormone levels reflect CIPOI in patients. Therefore, this pre-clinical mouse model is suitable for further exploration of the gut microbiota and its role in CIPOI.

As expected, there was significantly decreased alpha diversity and a significant distinction between beta diversity in mice with Cis-POI and control mice (Figures 1F, 1G, S1J, and S1K), which echoed our results in the human cohort. Subsequent analysis identified 11 genera that differed significantly between mice with Cis-POI and control mice (Figure 1H), including enrichment of *Lactobacillus*, *Roseburia*, and *Prevotella* in the control group,

(C) Correlation between alpha-diversity indices and serum hormone level. Spearman's rho statistic was adjusted using the Benjamini and Hochberg method. \* $p < 0.05$ .

(D) Significant microbial pathways associated with the differentially expressed microbial genes using over-representation analysis (ORA).

(E) Gut microbiota showed significantly different abundances between the CIPOI and Ctrl groups. Each point represents one species, and genera comprising over 10 species are displayed. The colors correspond to enrichment in CIPOI or Ctrl, and the circle sizes refer to the Log<sub>2</sub> fold change.

(F) Comparison of amplicon sequence variants (ASVs) between Cis and Ctrl mice. \* $p < 0.05$  by Wilcoxon rank-sum test.

(G) PCoA based on unweighted UniFrac distances revealed that the Ctrl bacterial communities clustered separately from the Cis bacterial communities. Each point represents a single sample, colored by group. Differences in beta diversity between Cis and Ctrl were tested by PERMANOVA.

(H) Linear discriminant analysis effect size identified the most differentially abundant taxa between the two groups. Ctrl-enriched genera are indicated with a positive linear discriminant analysis (LDA) score, and genera enriched in Cis controls had a negative score. Only taxa meeting an LDA significant threshold of  $>3$  are shown.

(I) Concordance of genus variations between the intestinal microbiota of the human and mouse model. The counts indicate the number of differential species in the human metagenome data.

(J–N) Relative abundance of *Lactobacillus* spp. of fecal samples from participants of the healthy group and the CIPOI group ( $N = 19$  for Ctrl and  $N = 21$  for CIPOI) (J) *L. reuteri*; (K) *L. plantarum*; (L) *L. fermenti*; (M) *L. buchneri*; (N) *L. delteri*.

(O–S) Relative abundance of *Lactobacillus* spp. of fecal samples from mice of the control group and the Cis-POI group ( $n = 8$  for Ctrl and  $n = 10$  for Cis-POI). (O) *L. reuteri*; (P) *L. plantarum*; (R) *L. fermenti*; (S) *L. buchneri*; (L) *L. delteri*. Data in (J)–(S) presented as the mean  $\pm$  SEM. \* $p < 0.05$ , \*\*\* $p < 0.001$ ; two-tailed Student's *t* test.

which paralleled observations in the human cohort (Figures 1I and S1L; Table S2). Considering there is evidence of protective effects of certain strains of *Lactobacillus* in preserving ovary<sup>21</sup> and alleviating chemotherapy-induced side effects,<sup>13,22,23</sup> we validated the change of the strains of *Lactobacillus* by quantitative PCR. In fecal samples from patients with CIPOI (Figures 1J–1N) and mice with Cis-POI (Figures 1O–1S), a significant decrease in the abundance of *Limosilactobacillus reuteri* was observed.

### The gut microbiota regulated ovarian toxicity induced by cisplatin

To determine whether the Cis-POI-related gut microbiota was associated with ovarian and hormonal damage, we performed fecal microbiota transplantation (FMT) to recipient mice with fecal bacterial suspension from mice with Cis-POI (Cis-FMT) or control animals (Ctrl-FMT) prior to cisplatin treatment to induce POI (Figure S2A). Oral administration of broad-spectrum antibiotics to deplete gut microbiota prior to FMT was performed using a well-established protocol.<sup>18</sup> When compared with FMT from Cis-POI mice (Cis+Cis-FMT) or cisplatin group (Cis), protective effects were observed for FMT from control mice (Cis+Ctrl-FMT). These effects included restoring the low weight of ovaries, increasing the serum concentration of E2, decreasing the serum concentration of FSH, normalizing the number of primordial and antral follicles, as well as reducing the number of atretic follicles and morphological damages on granulosa cells (Figures 2A–2D). Together, these results demonstrate that gut microbiota plays a role in the ovarian toxicity of cisplatin.

Based on these results, we proposed that the detrimental effect of CIPOI could also be restored by manipulating the gut environment. Therefore, we proposed that oral supplementation of *L. reuteri* in mice with Cis-POI would have beneficial effects (Figure S2B). Our results showed that supplementing Cis-POI mice with *L. reuteri* (*L. reuteri* DSM 1793) restored the low weight of ovaries and the serum concentration of E2, and high serum concentration of FSH as observed in Cis-POI mice without *L. reuteri* supplementation (Figures 2E, 2F, and S2C). In addition, *L. reuteri* pre-treatment in Cis-POI mice increased the number of primordial and antral follicles, reduced the number of atretic follicles and morphological damages on the ovary, and normalized the arrangement on granulosa cells (Figures 2G and 2H), indicating restoration in both follicle generation and development. Moreover, *L. reuteri* pre-treatment showed mitigation of antral follicular apoptosis in Cis-POI mice (Figure 2I). These findings demonstrate that supplementation of *L. reuteri* efficiently protected against experimental Cis-POI.

### The metabolite of gut microbiota, $\beta$ -RA, is downregulated in individuals with CIPOI

We next sought to understand the mechanism through which the gut microbiota asserts its modulatory effects on the pathogenesis of Cis-POI. We examined gut-derived metabolites, which form a crucial interface between gut bacteria and host health.<sup>24</sup> Fecal metabolomic analysis revealed that the composition of gut metabolites significantly differed between Cis-POI mice and controls (Figures 3A, 3B, and S3A). Cis-POI mice showed 42 enriched and 22 decreased metabolites when compared with

the control group (two-sided Wilcoxon rank-sum test,  $p < 0.05$ ,  $|\log_2FC| > 1$ , and variable influence on projection (VIP) value  $> 1$ ; Figure 3C). Interestingly, most of the differentially expressed metabolites in the Cis-POI group showed a positive correlation with the abundance of *Lactobacillus* (Figure 3C), indicating its potential involvement in the synthesis and degradation of disease-related metabolites. Additionally, our analysis revealed that one specific metabolite,  $\beta$ -resorcylic acid ( $\beta$ -RA, Figure S3B), demonstrated significant variations between the two groups, with notably reduced levels observed in the cecal and serum samples of Cis-POI mice as compared to the control group (Figure 3D). The same decrease in  $\beta$ -RA was also observed in fecal and serum samples from CIPOI participants when compared to healthy controls (Figure 3E).

To further investigate the relationship between gut microbiota and  $\beta$ -RA, we first depleted the gut microbiota using antibiotics. In antibiotic-treated mice, there was a significant reduction of  $\beta$ -RA compared to control mice (Figure 3F), indicating that gut bacteria play an important role in the generation of  $\beta$ -RA. Due to *L. reuteri* having a dominant protective effect, we tested whether this was through the generation of  $\beta$ -RA. Indeed, when cultured in de Man, Rogosa, and Sharpe agar (MRS) medium, *L. reuteri* (Figures S3C and S3D), as well as several other strains of *Lactobacillus*, were capable of producing  $\beta$ -RA (Figure S3E), so we sought to verify whether this was also reflected *in vivo*. Cis-POI mice with intragastric pre-treatment of *L. reuteri* resulted in significantly increased serum  $\beta$ -RA level (Figure 3G). Thus,  $\beta$ -RA may be a beneficial metabolite responsible for mediating the protective effect of *L. reuteri* on Cis-POI.

### $\beta$ -RA prevents cisplatin-induced ovarian damage

We next investigated whether  $\beta$ -RA could alleviate cisplatin-induced ovarian damage (Figure S4A). Cis-POI mice that received oral administration of  $\beta$ -RA were protected against disease-associated reductions in weights of ovaries and serum concentration of E2, and an increase in FSH (Figures 4A and 4B), confirming *in vivo* that  $\beta$ -RA administration conferred resistance to experimental cisplatin-induced ovarian injury. In addition, Cis-POI mice with  $\beta$ -RA pre-treatment showed increased numbers of primordial and antral follicles, and reduced numbers of atretic follicles and damage to the ovary structure, with a normalized arrangement of granulosa cells (Figures 4C and 4D), which was consistent with the protective effect of *L. reuteri* supplementation. Furthermore,  $\beta$ -RA pre-treatment in Cis-POI mice reduced apoptosis of antral follicles when compared with non-treated animals (Figure 4E). Next, we repeated these experiments under a germ-free condition to further investigate the dependency of gut microbiota in the protective effect of  $\beta$ -RA. Similarly, administration of  $\beta$ -RA protected against cisplatin-induced ovarian damage, including restoring the loss of ovarian weight, decreasing the number of primordial and antral follicles, and lowering the elevated level of FSH and the number of atretic follicles (Figures S4B–S4F). These results indicate that  $\beta$ -RA is capable of normalizing ovarian morphology and hormonal levels to protect against cisplatin-induced ovarian damage independent of gut microbiota.

Considering the biosorption of platinum-containing compounds by gut bacteria,<sup>25,26</sup> it is important to determine whether gut

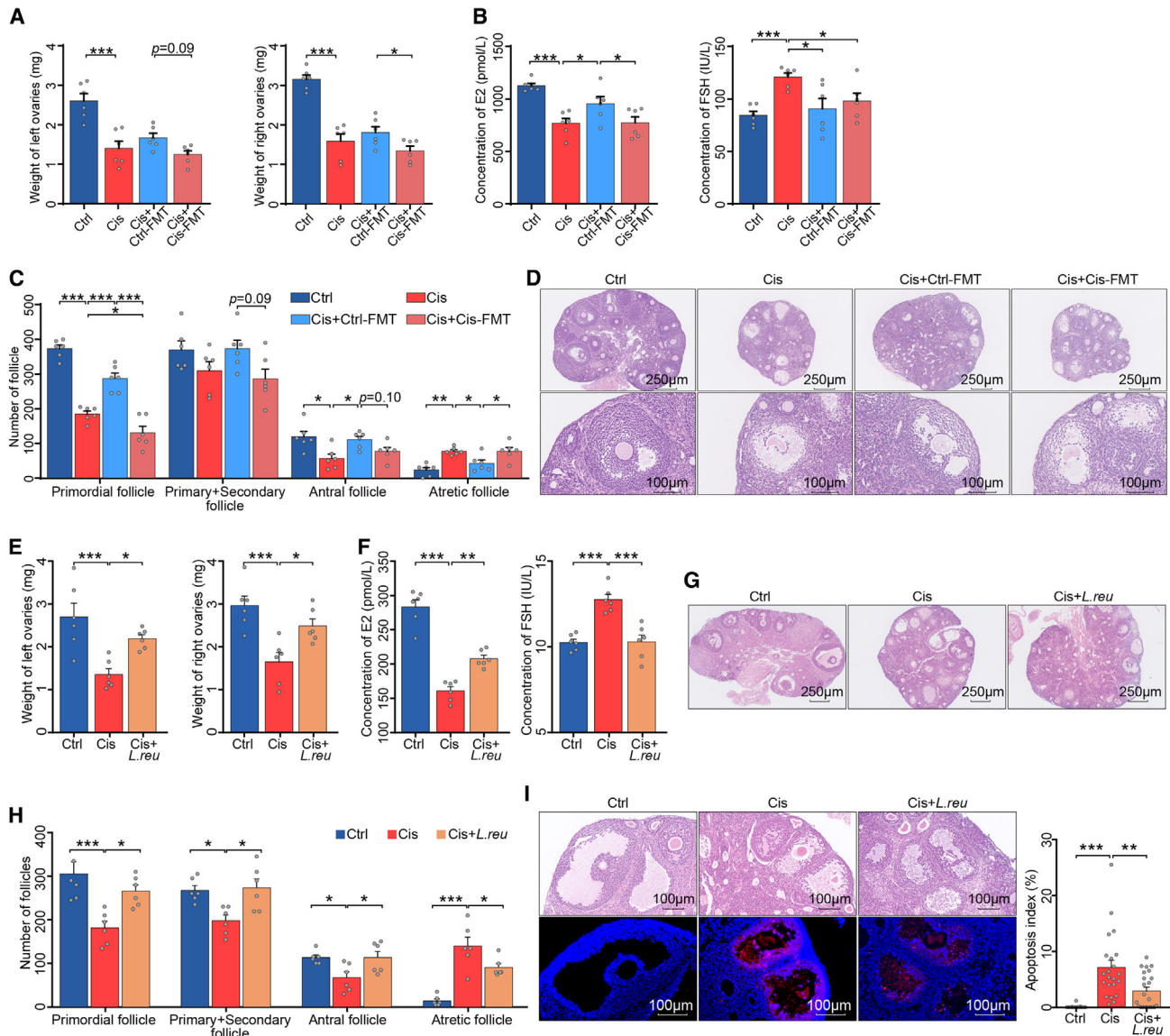


**Figure 2. The gut microbiota regulated ovarian toxicity induced by cisplatin**

(A) Ovarian weight of Ctrl, Cis, Cis+Ctrl-FMT, and Cis+Cis-FMT mice ( $n = 6$ ).  
 (B) Serum levels of E2 and FSH in Ctrl, Cis, Cis+Ctrl-FMT, and Cis+Cis-FMT mice ( $n = 6$ ).  
 (C) Quantification of primordial, primary + secondary, antral, and atretic follicles ( $n = 6$ ).  
 (D) Representative images of ovaries and antral follicles in recipient mice by H&E.  
 (E) Ovarian weight of Ctrl, Cis-POI, and Cis-POI+ *L. reuteri* mice ( $n = 6$ ).  
 (F) Serum levels of E2 and FSH in Ctrl, Cis-POI, and Cis-POI+ *L. reuteri* group ( $n = 6$ ).  
 (G) H&E staining of ovaries from mice in each group.  
 (H) Quantitative analysis of the primordial, primary + secondary, antral, and atretic follicles ( $n = 6$ ).  
 (I) Representative images of H&E-stained histological sections from antral follicles and TUNEL-based quantification of the apoptotic index in the antral follicles ( $n = 17$  for Ctrl,  $n = 21$  for Cis-POI, and  $n = 23$  for Cis-POI+*L. reuteri*). The data are all presented as the mean  $\pm$  SEM. \* $p < 0.05$ , \*\* $p < 0.01$ , \*\*\* $p < 0.001$ ; one-way ANOVA following the Benjamini and Hochberg's method for multiple adjustments in (A, B, and C); one-way ANOVA following the Dunnett's multiple comparisons test in (F, G, I, and J).

bacteria or microbes-derived metabolite administration would alter the pharmacodynamics of cisplatin. Thus, we performed pharmacokinetic experiments using mice with *L. reuteri* or  $\beta$ -RA prior to cisplatin treatment. Comparing with cisplatin-treated mice, we did not observe the statistical difference in the concen-

tration of cisplatin in mice with *L. reuteri* or  $\beta$ -RA treatment on the blood samples at 0, 15, 30, and 60 min, as well as 24, 48, and 72 h, and urine sample at 24, 48, and 72 h after cisplatin administration (Figures 4F–4I). These results indicate that neither  $\beta$ -RA nor *L. reuteri* would alter the metabolism and excretion of cisplatin in mice

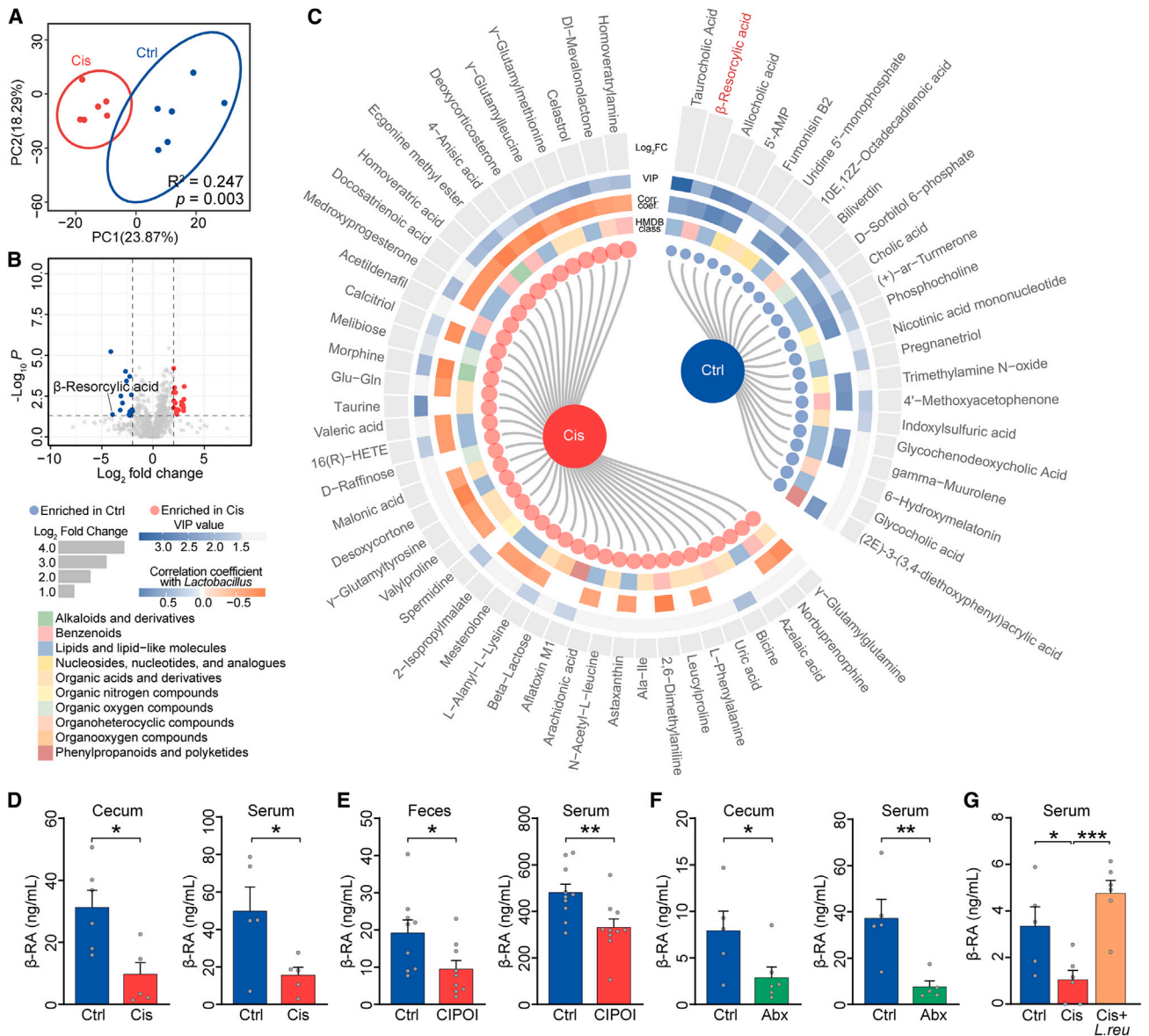


**Figure 3. The metabolite of gut microbiota,  $\beta$ -RA, is downregulated in individuals with CIPOI**

(A) Principal-component analysis of metabolites in samples from Cis mice (red points) and Ctrl mice (blue points). Permutational multivariate analysis of variance with the Bray-Curtis distance metric was used to assess the significance of differences between the two groups.

(B) Volcano plots of the metabolites. The data were compared using a two-tailed unpaired Student's t test.

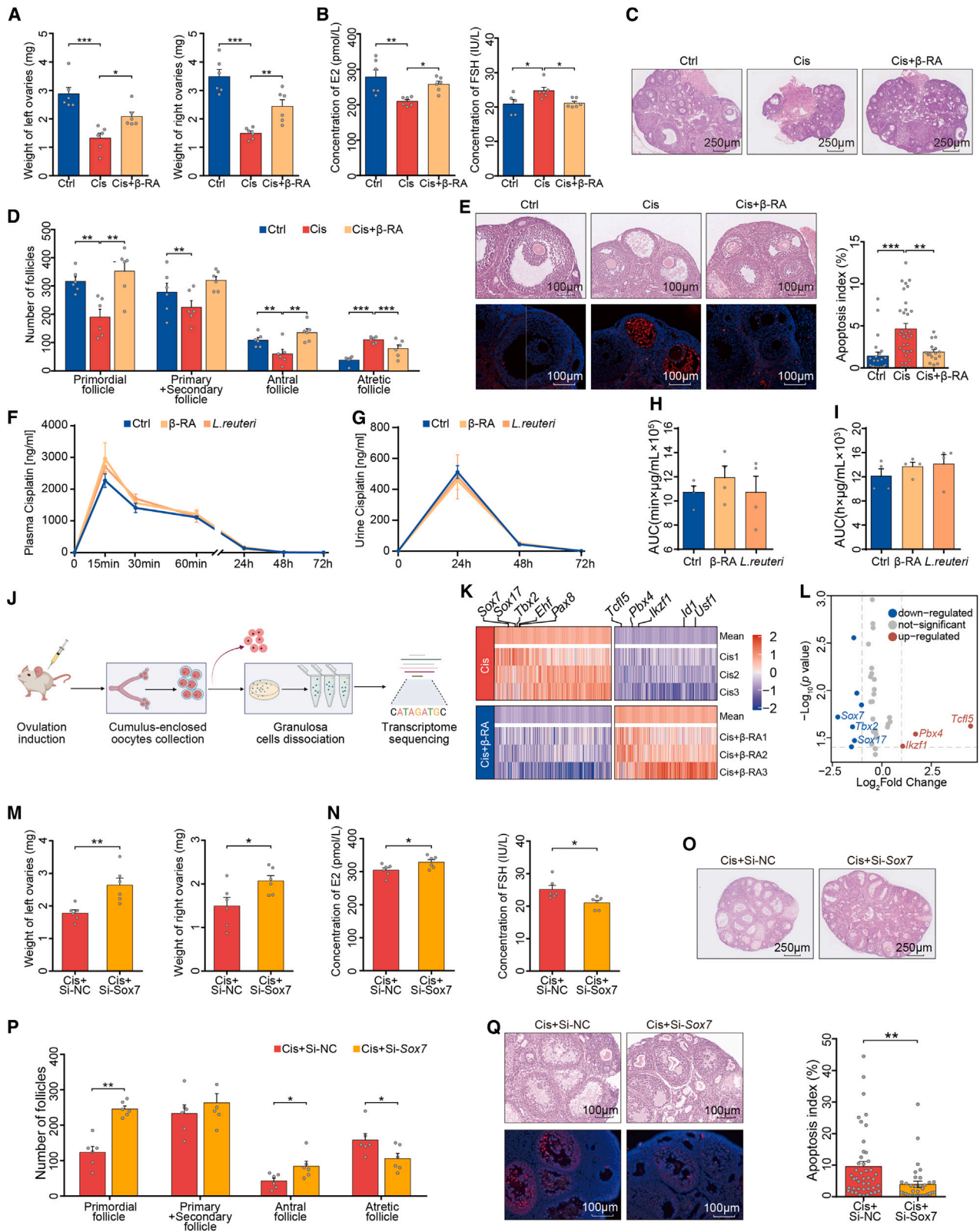
(C) The differential metabolites between Cis and Ctrl mice. Metabolites with VIP score  $>1$  and  $p$  value  $<0.05$  were significant. Blue points and red points in the internal cycle represent the enrichment in Ctrl and Cis mice, respectively. The second, third, and fourth inter-cycle represent the class of metabolites according to the Human Metabolome Database (HMDB) database, the correlation coefficient with *Lactobacillus*, and VIP scores, respectively. The external cycle shows the  $\text{Log}_2$  fold of change of each metabolite.

(D)  $\beta$ -RA levels in cecum content and serum from Ctrl and Cis-POI mice ( $n = 5$ ).

(E)  $\beta$ -RA levels in feces and serum from Ctrl and CIPOI women ( $n = 8$ ).

(F)  $\beta$ -RA levels in cecal content and serum of mice treated with or without antibiotics (Abx) ( $n = 5$ ).

(G)  $\beta$ -RA levels in serum from CIPOI mice treated with *L. reuteri* ( $10^9$  colony-forming units [CFUs] per day), gavaged to mice from 3 days before cisplatin exposure, and throughout the period of CIPOI modeling ( $n = 5$  for Ctrl,  $n = 6$  for Cis-POI, and Cis-POI+*L. reuteri*). The data are all presented as the mean  $\pm$  SEM. \* $p < 0.05$ , \*\* $p < 0.01$ , \*\*\* $p < 0.001$ ; Spearman's rho correlation in (C); two-tailed Student's t test in (D–F); one-way ANOVA following the Dunnett's multiple comparisons test in (G).



(legend on next page)

and, thus, are less likely to compromise the pharmacodynamics of cisplatin.

To further evaluate the effectiveness of *L. reuteri* and  $\beta$ -RA on Cis-POI under malignant conditions, we employed two tumor-bearing mouse models, including the Lewis lung carcinoma (LLC) and the ID8 ovarian cancer (OvCa), to explore the protective effects. In both LLC (Figure S5A-F) and OvCa (Figures S5G-S5L) mice treated with cisplatin, protective effects were observed for both *L. reuteri* and  $\beta$ -RA. These effects included restoring the low weight of ovaries; increasing the serum concentration of E2 (marginal significance in OvCa); decreasing the serum concentration of FSH; normalizing the number of primordial, preantral, and antral follicles; as well as reducing the number of atretic follicles and morphological damages on granulosa cells. In summary, the administration of *L. reuteri*, as well as  $\beta$ -RA, could alleviate the adverse effects of POI induced by cisplatin in OvCa and LLC model mice.

#### $\beta$ -RA reduces Sox7 level of granulosa cells linked to prevention of cisplatin-induced ovarian damage

Given that the maturation of an oocyte depends on the support of its surrounding granulosa cells,<sup>27,28</sup> we examined the effect of  $\beta$ -RA on granulosa cells as a pathway for protection against ovarian damage. Granulosa cells were extracted from the ovaries of Cis-POI mice with or without  $\beta$ -RA pre-treatment, and its transcriptome was analyzed (Figure 4J). There were significantly different gene expression profiles between granulosa cells isolated from  $\beta$ -RA-treated and untreated Cis-POI mice (Figures 4K and 4L). Notably, Gene Ontology analysis highlighted apoptosis as the dominant process that decreased due to  $\beta$ -RA treatment before cisplatin exposure (Figure S6A). The most enriched gene in Cis-POI mice with  $\beta$ -RA supplementation was sex-determining region Y-box 7 (*Sox7*), which has been reported to play a pivotal role in cellular apoptosis,<sup>29</sup> as well as vasculogenesis<sup>30</sup> and hematopoiesis.<sup>31</sup> Therefore,  $\beta$ -RA may have an antagonistic effect on SOX7 transcription. This is supported by our findings, using immunofluorescence and western blotting,

which showed that the SOX7 level in cisplatin-treated ovaries was significantly reduced with  $\beta$ -RA treatment (Figures S6B and S6C).

To determine the role of SOX7 in Cis-POI, we intravenously injected negative control- (NC-)small interfering RNA (siRNA) or *Sox7*-siRNA into mice prior to Cis-POI (Figure S6D). The knock-down efficiency was confirmed by real-time PCR (Figure S6E). As expected, genetic knockdown of murine *Sox7* led to a significant increase in ovarian weight, serum E2 concentration, as well as the number of the primordial and antral follicles in Cis-POI mice. Moreover, the administration of *Sox7*-siRNA decreased the serum concentration of FSH, the number of atretic follicles, and apoptosis of granulosa cells in the antral follicles (Figures 4M-4Q). Therefore, our results indicate that one mechanism through which  $\beta$ -RA prevents ovarian toxicity is by inhibiting SOX7 transcription, thereby suppressing apoptosis of granulosa cells.

#### Nuclear SOX7 induces granulosa cell apoptosis by binding to the Bax promoter

To explore the underlying mechanism of  $\beta$ -RA in preventing cisplatin-induced apoptosis of ovarian granulosa cells, we constructed an *in vitro* cell model derived from human granulosa-like tumor cells (KGN cells) to mimic the impact of  $\beta$ -RA in cisplatin-induced damages. The proportion of apoptotic cells was markedly reduced by  $\beta$ -RA treatment, as assessed by flow cytometry with Annexin V/PI staining and TUNEL assay (Figures S6F and S6G). In addition,  $\beta$ -RA treatment significantly improved the proliferation rate of KGN cells with cisplatin exposure (Figure S6H). Given that Bcl-2-associated X (BAX) serves as a key initiator of apoptosis,<sup>32</sup> whereas BCL2 protein is more functionally characterized as an anti-apoptotic factor, we measured BAX and BCL2 expression in KGN cells. As expected,  $\beta$ -RA treatment reduced the mRNA expression level of *Bax* in KGN cells with cisplatin exposure (Figure S6I), which was mirrored at the protein level through substantially reduced BAX/BCL2 ratio and SOX7 expression (Figure S6K).

#### Figure 4. $\beta$ -RA prevents cisplatin-induced ovarian damage by suppressing granulosa cell apoptosis

- (A) Ovarian weight of Ctrl, Cis-POI, and Cis-POI+ $\beta$ -RA mice ( $n = 6$ ).  
 (B) Serum levels of E2 and FSH of mice in each group ( $n = 6$ ).  
 (C) H&E staining of ovaries from Ctrl, Cis-POI, and Cis-POI+ $\beta$ -RA group.  
 (D) Quantification of the primordial, primary + secondary, antral, and atretic follicles ( $n = 6$ ).  
 (E) Representative images of antral follicles in recipient mouse ovaries by H&E staining and TUNEL-based quantification of apoptotic index in antral follicles (23, 32, and 16 antral follicles from five independent sections of Cis and Cis+ $\beta$ -RA group, respectively).  
 (F-I) Measurement of serum and urine cisplatin concentration in mice given *L. reuteri* and  $\beta$ -RA 3 consecutive days and followed by a single injection of 1.5 mg/kg cisplatin via an intraperitoneal route. (F) Concentration of cisplatin in plasma at 0, 15, 30, and 60 min and 24, 48, and 72 h after cisplatin exposure. ( $n = 4$ ) (G) Concentration of cisplatin in urine at 0, 24, 48, and 72 h after cisplatin administration. ( $n = 4$ ) (H) The area under the plasma concentration-time curve (AUC) from time zero to the time last measurable plasma concentration ( $n = 4$ ). (I) The area under the urine concentration-time curve (AUC) from time zero to the time last measurable plasma concentration ( $n = 4$ ).  
 (J) Experimental design for ovarian granulosa cell isolation and transcriptome analysis.  
 (K) Heatmap analysis of gene expression profiles of ovarian granulosa cells. The top five differential genes are shown ( $n = 3$ ).  
 (L) Volcano plot showing the top three deficient transcription factors.  
 (M) Ovarian weight of Cis+Si-NC and Cis+Si-*Sox7* mice ( $n = 6$ ).  
 (N) Serum levels of E2 and FSH of Cis-POI mice ( $n = 6$ ).  
 (O) H&E staining of ovaries from Cis-POI mice treated with or without *Sox7*-siRNA.  
 (P) Quantitative analysis of primordial, primary + secondary, antral, and atretic follicles ( $n = 6$ ).  
 (Q) Representative images of H&E-stained histological sections of antral follicles and TUNEL-based quantification of the apoptotic index in antral follicles (44 and 34 antral follicles from five independent sections of Cis+Si-NC and Cis+Si-*Sox7* group, respectively). The data are all presented as the mean  $\pm$  SEM. \* $p < 0.05$ , \*\* $p < 0.01$ , \*\*\* $p < 0.001$ ; one-way ANOVA following the Dunnett's multiple comparisons test in (A, B, D, E, H, and I); two-tailed Student's *t* test in (M, N, P, and Q).

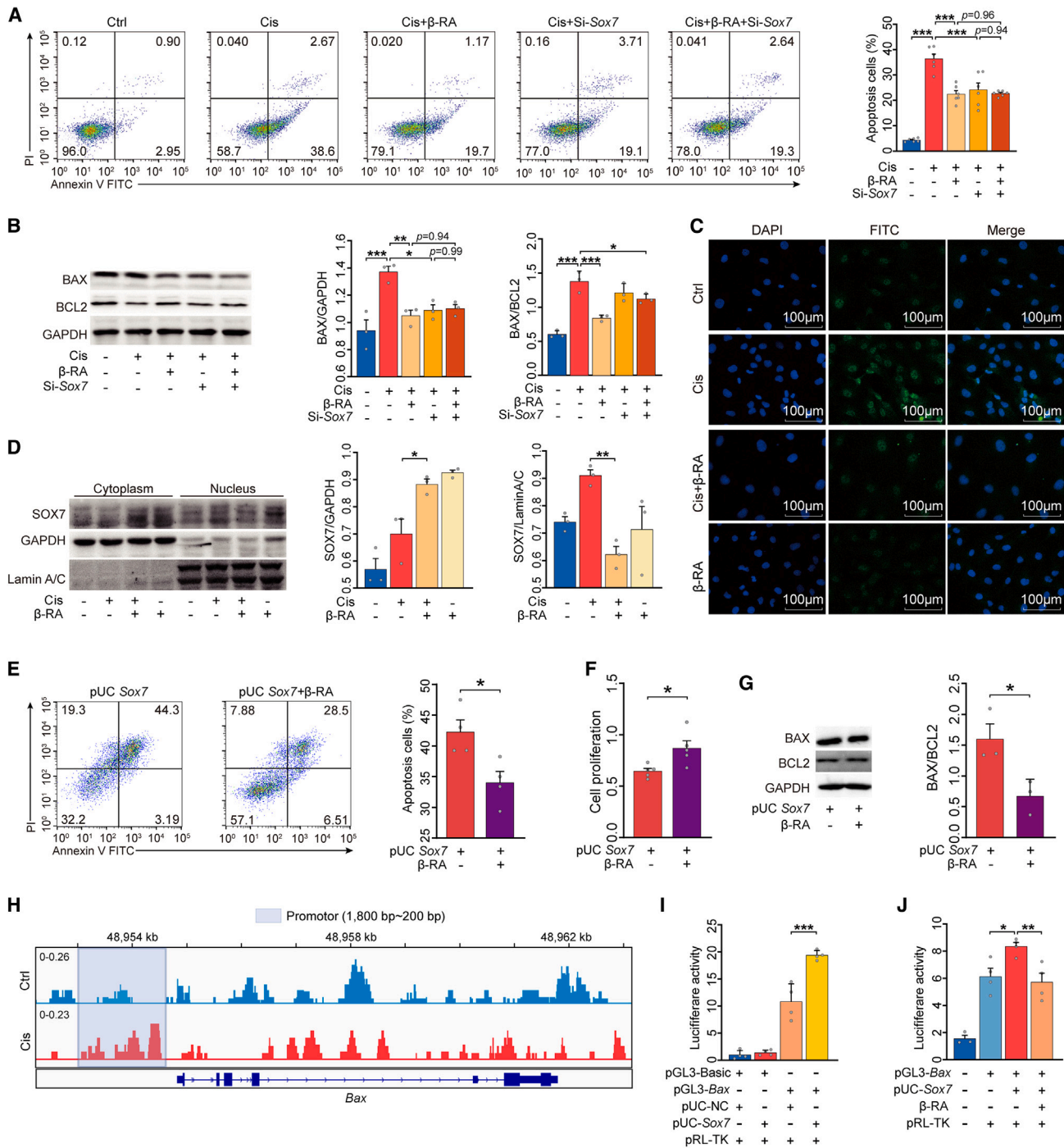


**Figure 5. Nuclear SOX7 induces granulosa cell apoptosis by binding to the Bax promoter**

- (A) Flow cytometric analysis of the proportion of apoptotic KGN cells ( $n = 6$ ).  
 (B) Western blotting of BAX and BCL2 and their quantification ( $n = 3$ ).  
 (C) Representative immunofluorescence images of SOX7 expression in KGN cells. Green represents SOX7 while blue represents DAPI.  
 (D) Western blotting was performed to quantify SOX7 expression in the nucleus and cytoplasm ( $n = 3$ ).  
 (E) The proportion of apoptotic KGN cells was determined using Annexin V-fluorescein isothiocyanate (FITC)/propidium iodide (PI) staining and flow cytometry ( $n = 4$ ).  
 (F) Cell Counting Kit-8 was used to measure the relative cell viability ( $n = 5$ ).  
 (G) Representative western blot analysis of BAX and BCL2 from the lysis solution of KGN cells ( $n = 3$ ).

(legend continued on next page)

Next, based on the potential interaction between SOX7- and BAX-mediated apoptosis, we constructed an *Sox7* knockdown granulosa cell line derived from human KGN cells to confirm the role of *Sox7* on granulosa cell apoptosis. Both *Sox7* knockdown and  $\beta$ -RA treatment significantly reduced the proportion of apoptotic cells and increased the proliferation of granulosa cells challenged with cisplatin (Figures 5A and S6J), in addition to cisplatin-mediated elevation in BAX level (Figure 5B). However, there was no combined effect of  $\beta$ -RA treatment and *Sox7* knockdown on apoptosis, proliferation, or BAX levels. Considering that SOX7 has been shown to translocate from the cytosol to the nuclei,<sup>33</sup> we utilized immunofluorescence and nucleocytoplasmic separation to determine whether  $\beta$ -RA directly decreases the cisplatin-induced nuclear accumulation of SOX7 in granulosa cells. As expected,  $\beta$ -RA treatment inhibited SOX7 nuclear levels in granulosa cells challenged with cisplatin (Figures 5C and 5D). Conversely, overexpression of *Sox7* in the same cell line allowed  $\beta$ -RA treatment to reduce the percentage of apoptotic cells, elevate cell proliferation, and decrease the BAX/BCL2 ratio (Figures 5E–5G, S6L, and S6M).

We then performed a genome-wide chromatin immunoprecipitation (ChIP) assay using a specific SOX7 antibody to determine the in-nucleus function of SOX7 and whether the expression of *Bax* was mediated by the interactions with SOX7. We found that SOX7 directly bound to the promoter region of *Bax* in KGN cells (Figure 5H). In a luciferase activity assay, overexpression of *Sox7* significantly increased *Bax* promoter-driven luciferase activity (Figure 5I). Finally, in the granulosa cells challenged with cisplatin, the transcriptional activity of the *Bax* promoter was markedly decreased with  $\beta$ -RA administration (Figure 5J). Collectively, our findings demonstrate that  $\beta$ -RA inhibits the nuclear accumulation of SOX7 and suppresses the activity of BAX to inhibit apoptosis of granulosa cells.

### $\beta$ -RA supplementation improved the fertilization and fertility deficits induced by cisplatin in mice

In addition to the important role of  $\beta$ -RA in regulating apoptosis of granulosa cells, we also investigated whether  $\beta$ -RA had protective effects on the development of oocytes and the *in vivo* capacity for fertilization. Considering the time from primordial follicle activation to ovulation is about 2–3 weeks in mice,<sup>34</sup> we isolated oocytes from mice 2 weeks after the completion of Cis-POI mouse model construction. Pre-treatment of Cis-POI mice with  $\beta$ -RA elevated the number of ovulated oocytes in superovulation (Figures 6A and 6B) and improved the meiotic progression of oocytes, indicated by the higher rate of first polar body extrusions (Figures 6A and 6C). The reproductive process involves several stages, including the formation of a functional zygote, the development of an embryo, and the growth of a fetus. Successful reproduction requires the completion of all stages.

To assess fertility, we performed an *in vitro* fertilization experiment in mice and observed that  $\beta$ -RA pre-treatment significantly increased the number of sperm binding to the zona pellucida, which was reduced in Cis-POI mice (Figures 6D and 6E). In addition,  $\beta$ -RA pre-treatment significantly reverted cisplatin-induced low 2-cell embryo formation rate and morula formation rate of fertilized oocytes, indicating its capability in rescuing fertilization and early embryonic development of fertilized oocytes from Cis-POI (Figures 6F–6I). These results demonstrate that  $\beta$ -RA improved the function of oocytes, leading to successful fertilization and subsequent embryonic development.

Moreover, we tested the potential of  $\beta$ -RA supplementation in improving the reproductive function of Cis-POI mice. Thirty mice with Cis-POI were randomly assigned to two groups either with or without  $\beta$ -RA pre-treatment. The mice in each group were mated with untreated fertile males at 2 weeks post-cisplatin. Four out of 15  $\beta$ -RA pre-treated Cis-POI mice successfully conceived and delivered, while no pregnancy was observed in Cis-POI mice without  $\beta$ -RA supplement (Figure 6J). After delivery, the mice in the postnatal period as well as the mice who fail to conceive were then mated for a second round to assess their reproductive function. Although recovery in reproductive function in both groups was observed, Cis-POI mice with  $\beta$ -RA pre-treatment showed a significant increase in both the number and weight of pups compared with those without  $\beta$ -RA pre-treatment (Figures 6K–6M). Taken together, our results indicate that  $\beta$ -RA pre-treatment alleviates cisplatin-induced damage on oocytes, restores their maturation process and reproductive function, and rescues the consequent subfertility caused by Cis-POI.

## DISCUSSION

The adverse effects of chemotherapeutic damage, including hormone deficiency, loss of ovarian reserves, and the consequential detriment on quality of life and fertility, have long been recognized.<sup>35</sup> Women diagnosed with cancer and subsequently commencing treatment are 38% less likely to conceive compared to healthy women, with all diagnostic groups of cancer and all groups by age contributing to this reduction.<sup>36</sup> In light of this situation, there is now a pressing need to develop methods to protect patients from the damaging effects of chemotherapy on the reproductive system. As cisplatin-based combination chemotherapy is considered the standard first-line treatment for multiple cancers<sup>19</sup> with gonadotoxicity,<sup>20</sup> we recruited CIPOI patients under cisplatin-based treatment and constructed a cisplatin-induced mouse model to study the capability of gut microbes and gut-derived metabolites to reverse infertility. We identified a gut-derived metabolite,  $\beta$ -RA, which could ameliorate hormone deficiency, improve the quantity and quality of follicles, rescue zygote development, and increase

(H) Chromatin from KGN cells treated with or without cisplatin was collected for immunoprecipitation with SOX7 antibody. The Integrative Genomics Viewer (IGV) track of the input-subtracted SOX7 chromatin immunoprecipitation sequencing (ChIP-seq) signal at the promoter of the *Bax* gene (200–1,800 bp) is displayed.

(I) The effect of *Sox7* overexpression on *Bax* transcriptional activity. KGN cells were co-transfected with pGL3-basic vector or pGL3-*Bax*, pUC-NC, or pUC-*Sox7* along with the pRL-TK plasmid and cultured for 48 h. Luciferase activity was detected and normalized to Renilla (RL) activity ( $n = 4$ ).

(J) KGN cells were transfected with pGL3-*Bax* and pUC-*Sox7* for 48 h. KGN cells were then treated with or without  $\beta$ -RA for 6 h. Relative luciferase activity in each group ( $n = 4$ ). The data are all presented as the mean  $\pm$  SEM. \* $p < 0.05$ , \*\* $p < 0.01$ , \*\*\* $p < 0.001$ ; one-way ANOVA following the Dunnett's multiple comparisons test in (A, B, D, I, and J); two-tailed Student's *t* test in (E–G).

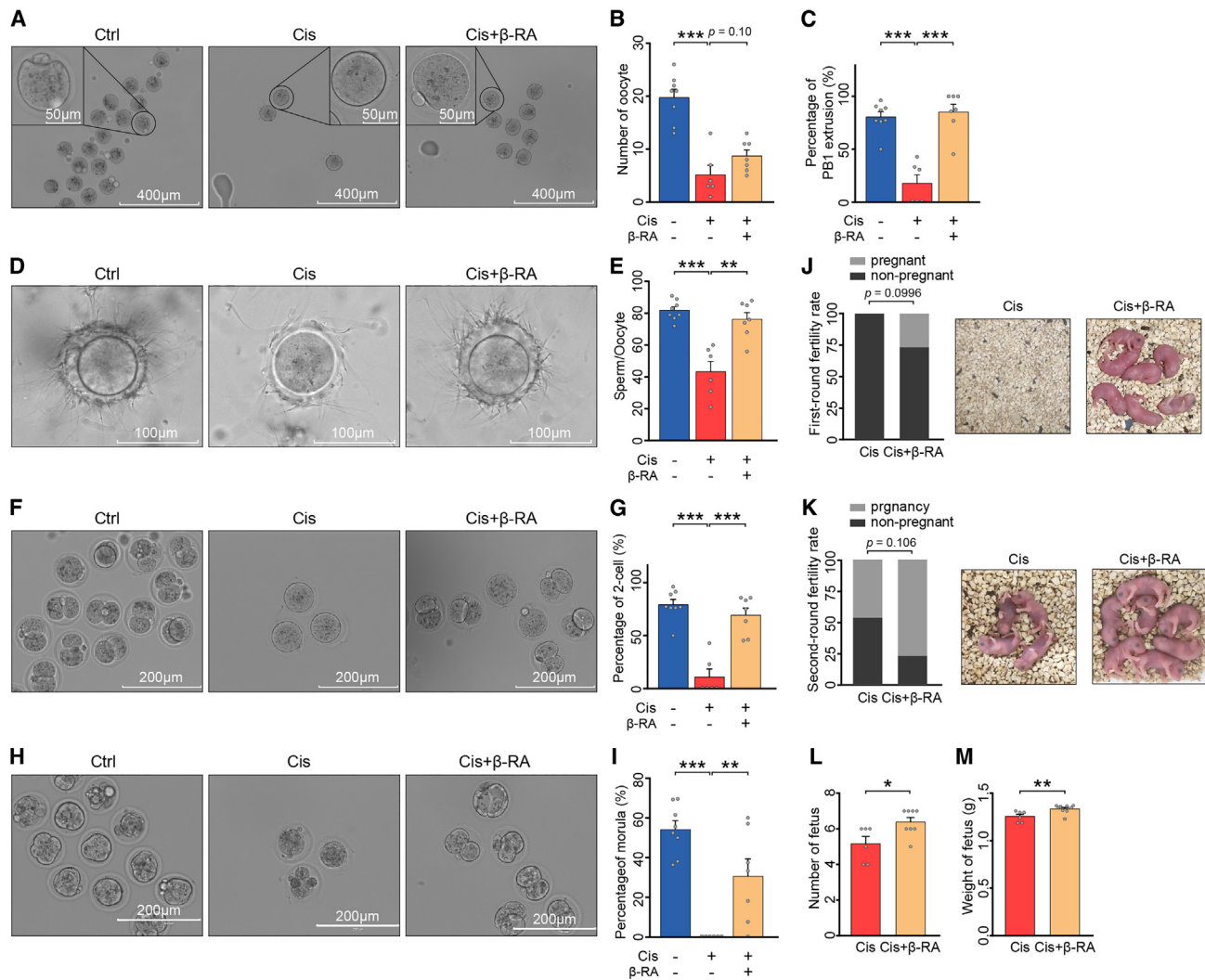


**Figure 6.  $\beta$ -RA supplementation improved the fertilization and fertility deficits in cisplatin-treated mice**

(A) Representative photomicrographs of *in vivo*-matured oocytes collected from control, Cis-POI, and Cis-POI+ $\beta$ -RA mice. Scale bar: 400  $\mu$ m and 50  $\mu$ m. (B) Ovulated oocytes were counted in control ( $n = 8$ ), Cis-POI ( $n = 6$ ), and Cis-POI+ $\beta$ -RA ( $n = 7$ ) mice. (C) The rate of the first polar body extrusion (PBE) was recorded in control ( $n = 8$ ), Cis-POI ( $n = 6$ ), and Cis-POI+ $\beta$ -RA ( $n = 7$ ) mice oocytes. (D–M) Protective effect of  $\beta$ -RA on fertilization and fertility in Cis-POI mice. (D) Representative image of sperm binding to zona pellucida of control ( $n = 8$ ), Cis-POI ( $n = 6$ ), and Cis-POI+ $\beta$ -RA ( $n = 7$ ) oocytes. Scale bar: 100  $\mu$ m. (E) The sperm binding to the surface of the zona pellucida surrounding oocytes from the control ( $n = 8$ ), Cis-POI ( $n = 6$ ), and Cis-POI+ $\beta$ -RA ( $n = 7$ ) groups was counted. (F and H) Representative image 2-cell (F) and morula (H) of control ( $n = 8$ ), Cis-POI ( $n = 6$ ), and Cis-POI+ $\beta$ -RA ( $n = 7$ ) oocytes. Scale bar: 200  $\mu$ m. (G) The percentage of 2-cell embryos was recorded in the control ( $n = 8$ ), Cis-POI ( $n = 6$ ), and Cis-POI+ $\beta$ -RA ( $n = 7$ ) groups. (I) The percentage of morula was recorded in the control ( $n = 8$ ), Cis-POI ( $n = 6$ ), and Cis-POI+ $\beta$ -RA ( $n = 7$ ) groups. (J) Percentage of pregnant mice in the first round between Cis-POI and Cis-POI+ $\beta$ -RA was compared using Fisher's exact test. (K) Percentages of pregnant mice in the second round between Cis-POI and Cis-POI+ $\beta$ -RA were compared using Fisher's exact test. (L and M) The fertility of Cis-POI ( $n = 6$ ) and Cis-POI+ $\beta$ -RA ( $n = 8$ ) mice was assessed by mating with male mice in the second round and recording the cumulative number (L) and weight of pups (M). The data are all presented as the mean  $\pm$  SEM. \* $p < 0.05$ , \*\* $p < 0.01$ , \*\*\* $p < 0.001$ ; one-way ANOVA following the Dunnett's multiple comparisons test in (B, C, E, G, and I); Fisher's exact test in (J and K); two-tailed Student's t test in (L and M).

the conception and delivery rate after cisplatin treatment. Moreover, we also reported a mechanism by which  $\beta$ -RA rescued granulosa cell apoptosis via the SOX7-BAX axis, which supported the development of oocytes combined with the restored hormone status. Our findings indicate a “gut-ovary axis” and offer a perspective to protection against cisplatin-induced damage in the human ovary.

There is currently no information available on the relationship between female reproductive functions and gut microbiota change during platinum-compound therapy. We assessed the bacterial profiles in both patients with Cis-POI and a Cis-POI mouse model. Our study showed that FMT using feces derived from mice with cisplatin treatment led to more severe cisplatin-induced gonadotoxicity than FMT from control mice. Moreover,

based on the previous studies demonstrating the protective effect of gut bacteria in cisplatin-induced adverse effects,<sup>37–39</sup> we demonstrated the therapeutic effect of a probiotic, *L. reuteri*, in restoring reproductive function after cisplatin treatment. As *Lactobacillus*-based probiotic was previously shown to provide a renal protective effect in cisplatin-treated rats (*L. reuteri*)<sup>37</sup> and the enhancement of cisplatin antitumor effect (*L. acidophilus*),<sup>40</sup> our study further showed the therapeutic effect of *L. reuteri* in cisplatin-induced reproductive system damage. Furthermore, we reported that a microbiota-derived metabolic product,  $\beta$ -RA, confers a preservative effect in cisplatin-induced fertility impairment. It is noteworthy that  $\beta$ -RA, as a catabolite of *L. reuteri*, could also be produced by other strains of *Lactobacillus* and potentially a variety of other bacteria.  $\beta$ -RA has also been reported to have a protective effect on renal and neural injury.<sup>41–43</sup> The results presented in this study further demonstrate its capability to alleviate cisplatin-induced gonadotoxicity and improve the development of the follicle and subsequent fertility, which deepens our understanding of profiles of the gut microbiota and microbiota-derived metabolic products in Cis-POI and provides a path toward fertility preservation after cisplatin treatment. Moreover, the pharmacokinetic analysis demonstrated that the  $\beta$ -RA treatment would not alter the metabolism and excretion of cisplatin, suggesting that it would not compromise the anticancer efficacy of cisplatin. Our germ-free mice experiments showed that the protective effects of  $\beta$ -RA were independent of gut microbiota, providing evidence that  $\beta$ -RA is potentially the final product of gut microbial-derived metabolite that preserved the ovary. Taken together, our study provides evidence that a microbes-derived metabolite,  $\beta$ -RA, alleviated cisplatin-induced damages in the ovarian tissue, thereby enhancing the ovarian reserve and function and preventing POI. These findings indicate the potential of  $\beta$ -RA for clinical translation.

In a normal state of folliculogenesis, follicles are developed from the primordial follicles with non-proliferative pre-granulosa cells to growing follicles surrounded by differentiated granulosa cells; at this point, one follicle is selected for dominance and ovulation.<sup>44</sup> Folliculogenesis mainly involves two essential co-dependent components: the oocyte and the surrounding granulosa cells. The maturation of oocytes critically relies on the support of granulosa cells to perform essential functions including glucose and lipid metabolism, energy supply, and meiotic regulation.<sup>45</sup> Due to the high proliferation rate, granulosa cells in the growing follicle undergo apoptosis and render themselves a key site for the adverse effects of gonadotoxic chemotherapy.<sup>20,46,47</sup> Also, apoptosis is observed in cells ranging from dormant to growing oocytes.<sup>20</sup> The deterioration of functional follicle units, therefore, impairs the possibility of successful conception. In the present study, we showed that both *L. reuteri* and  $\beta$ -RA could increase the number of primordial follicles and alleviate the apoptosis of granulosa cells in cisplatin-treated mice. The growing body of evidence suggests that granulosa cell apoptosis is a major cause of follicular atresia and dysregulated hormone secretion.<sup>48,49</sup> Combined with our observation of reductions in atretic follicles, this indicates that the protective effect might be achieved by guarding the follicle development process. We propose that *L. reuteri* and  $\beta$ -RA could be high-potential therapeutic targets in the alleviation of cisplatin-

induced follicular damage. Moreover, a central question in treating cisplatin-induced infertility is determining how to increase the number of available high-quality oocytes. The damage of chemotherapy to the reproductive system is comprehensive and affects reproductive organs, including the ovary and uterus.<sup>50</sup> In addition to the ovulation of a high-quality follicle, successful reproduction requires all conditions to be satisfied in the reproductive process, from a functional zygote to an embryo and ultimately to a fetus. Successful fertilization and subsequent embryonic development are prerequisites for the material basis for the onset of life.<sup>51</sup> Multiple factors could affect the outcome of fertility, including the quality and quantity of oocytes, ovum attraction to sperm, formation of morula, implantation in the uterus, and successful delivery. Therefore, the evaluation of follicles alone is insufficient to reflect the impact of treatment on fertility. In the present study, we further demonstrated the preservative effect of  $\beta$ -RA throughout the reproductive process, from fertilization rate and early embryonic development of fertilized oocytes to successful delivery rate and the characteristics of pups. Although we only assessed the protective mechanism of  $\beta$ -RA in the formation of follicles, nevertheless, it is noteworthy that the therapeutic effects of  $\beta$ -RA throughout the whole reproductive process imply the potential capability to rescue damage to the whole reproductive system, including the ovaries (manifested as maturation of follicle and subsequential fertilization) and uterus (manifested as the successful delivery). Therefore, a direction for future study could be to elucidate the effects of  $\beta$ -RA on the uterus, including egg imbedding and hematopoietic specification, as well as the underlying mechanisms.

We also found a pathogenic role of SOX7 in promoting granulosa cell apoptosis and damaging the ovaries, which could be negatively regulated by  $\beta$ -RA. As a nuclear transcription factor, SOX7 plays an important role in attenuating cancer cell apoptosis through the upregulation of pro-apoptotic genes associated with the p38 and extracellular signal-regulated kinases (ERK) signaling pathways.<sup>29,30</sup> In the present study, we identified SOX7 as a positive regulator of apoptosis in granulosa cells and found that knockdown of its expression has potential therapeutic benefits for Cis-POI. We further demonstrated the mechanism by which SOX7 induces an apoptotic effect on granulosa cells. SOX7 translocated from the cytoplasm into the nucleus to bind to the promoter region of *Bax* and upregulated transcriptional activity, culminating in the activation of apoptosis. The beneficial effects of reducing follicular atresia by inhibiting *Sox7* were also confirmed in mice experiments with RNA interference. Additionally, our data revealed that  $\beta$ -RA is an inhibitor of SOX7 expression. Future investigations are needed to elucidate in detail the mechanism by which  $\beta$ -RA inhibits SOX7 expression.

In summary, our findings provide insights into how gut dysbiosis is involved in the follicle depletion by promoting SOX7 interactions with the *Bax* promoter region in the nucleus, thereby priming apoptosis of granulosa cells and increasing host susceptibility to ovarian injury. These findings highlight the significance of the  $\beta$ -RA/SOX7/BAX axis mediated by *L. reuteri* in ovarian damage, shedding light on promising therapeutic strategies for Cis-POI. Modulating gut microbiota, specifically through *L. reuteri* and  $\beta$ -RA, could be of therapeutic importance in treating Cis-POI.

### Limitations of the study

There are several limitations to this study. Firstly, since the design of the study was exploratory and proof of concept, the cohort was relatively small despite adjustments accommodating BMI and age, which might still lead to bias in gut microbiota results. Future studies on a larger population are required to provide a more comprehensive gut bacterial interpretation, as well as the long-term safety and generalizability of  $\beta$ -RA. Secondly, we only recruited patients with POI after cisplatin-based treatment and used Cis-POI mice in our study. Although a number of common chemotherapy agents, including cisplatin, cyclophosphamide, and doxorubicin, could induce apoptosis of granulosa cells which leads to damage to oocyte development following follicle disruption,<sup>20,52</sup> whether the gut microbiota and  $\beta$ -RA exert protective effects on other chemotherapy agents requires further validation. Thirdly, while our study revealed that both gut microbiota and  $\beta$ -RA have the potential to rescue primordial follicles, further research is necessary to understand the underlying mechanism of this observation, as primordial follicles play a crucial role in the formation of functional follicles.<sup>53</sup> The relationship between primordial follicles and both gut microbiota and gut bacteria-derived metabolites should be deduced, as well as the underlying protective mechanisms, from primordial follicle formation through to subsequent ovulation.

### STAR★METHODS

Detailed methods are provided in the online version of this paper and include the following:

- KEY RESOURCES TABLE
- RESOURCE AVAILABILITY
  - Lead contact
  - Materials availability
  - Data and code availability
- EXPERIMENTAL MODEL AND SUBJECT DETAILS
  - Patients and clinical specimens
  - Murine studies
  - Bacterial strains and growth condition
  - Cell lines
- METHOD DETAILS
  - Sequencing and analysis
  - Histological analysis and follicular count
  - TUNEL staining
  - Transmission electron microscopy (TEM)
  - ELISA
  - *In vivo* pharmacokinetic study
  - Liquid chromatography/mass spectrometry
  - Superovulation, oocytes collection and granulosa cell isolation
  - *In vitro* fertilization and embryo culture
  - Transcriptome resequencing and analysis
  - Cell stimulation and transfections
  - Cell proliferation assay
  - Cell apoptosis
  - Quantitative reverse-transcription PCR
  - Immunofluorescence
  - Western blot
  - Nuclear and cytoplasmic separation
  - ChIP-seq analysis
  - Dual-luciferase reporter gene system
- QUANTIFICATION AND STATISTICAL ANALYSIS

### SUPPLEMENTAL INFORMATION

Supplemental information can be found online at <https://doi.org/10.1016/j.xcrm.2024.101678>.

### ACKNOWLEDGMENTS

This work was supported by the National Natural Science Foundation of China (82101721 [Xia Chen], 82371649 [Xia Chen], 82201812 [H.Z.], and 82260303 [C.Y.]), the China Postdoctoral Science Foundation (2023T160108 [Huimin Zheng] and 2022M710696 [H.Z.]), the Natural Science Foundation of Guangdong Province (2022A1515110278 [H.Z.], 2021A1515110183 [Y.F.], 2020A1515110321 [Xia Chen], and 2022A1515140128 [Xia Chen]), and the Medical Scientific Research Foundation of Guangdong Province (A2022277 [Xia Chen]). The funding bodies had no role in the study design, data collection or analysis, decision to publish, or preparation of the manuscript.

### AUTHOR CONTRIBUTIONS

Xia Chen, Y.F., P.L., and G.C. were responsible for the study design, supervision, and manuscript preparation; Y.F., J.C., S. Zhang, F.M., Z.L., M.Z., R.W., Z.M., and S.G. were responsible for the experiment; P.L., Y.F., H.Z., Z.W., W.T., Z.L., and R.Z. were responsible for statistical and bioinformatic analyses; C.Y., X.H., R.Z., Q.H., D.L., W.L., Y.H., and S. Zheng were responsible for the collection of human samples and clinical data. P.L., Y.F., S.S., T.J., H.Z., and Xueqin Chen drafted the manuscript and contributed to the interpretations of the findings and the critical revision of the manuscript. Y.Y. and E.M.E.-O. revised the manuscript for important intellectual content. All authors provided critical revisions and approved the final manuscript.

### DECLARATION OF INTERESTS

The authors declare no competing interests.

Received: May 8, 2024

Revised: June 7, 2024

Accepted: July 11, 2024

Published: August 2, 2024

### REFERENCES

1. van Dorp, W., Haupt, R., Anderson, R.A., Mulder, R.L., van den Heuvel-Eibrink, M.M., van Dulmen-den Broeder, E., Su, H.I., Winther, J.F., Hudson, M.M., Levine, J.M., and Wallace, W.H. (2018). Reproductive Function and Outcomes in Female Survivors of Childhood, Adolescent, and Young Adult Cancer: A Review. *J. Clin. Oncol.* 36, 2169–2180. <https://doi.org/10.1200/JCO.2017.76.3441>.
2. Ugai, T., Sasamoto, N., Lee, H.Y., Ando, M., Song, M., Tamimi, R.M., Kawachi, I., Campbell, P.T., Giovannucci, E.L., Weiderpass, E., et al. (2022). Is early-onset cancer an emerging global epidemic? Current evidence and future implications. *Nat. Rev. Clin. Oncol.* 19, 656–673. <https://doi.org/10.1038/s41571-022-00672-8>.
3. Gupta, S., Harper, A., Ruan, Y., Barr, R., Frazier, A.L., Ferlay, J., Steliarova-Foucher, E., and Fidler-Benaoudia, M.M. (2020). International Trends in the Incidence of Cancer Among Adolescents and Young Adults. *J. Natl. Cancer Inst.* 112, 1105–1117. <https://doi.org/10.1093/jnci/djaa007>.
4. Carson, S.A., and Kallen, A.N. (2021). Diagnosis and Management of Infertility: A Review. *JAMA* 326, 65–76. <https://doi.org/10.1001/jama.2021.4788>.
5. De Vos, M., Devroey, P., and Fauser, B.C. (2010). Primary ovarian insufficiency. *Lancet* 376, 911–921. [https://doi.org/10.1016/S0140-6736\(10\)60355-8](https://doi.org/10.1016/S0140-6736(10)60355-8).
6. Dyer, S.J., and Patel, M. (2012). The economic impact of infertility on women in developing countries - a systematic review. *Facts Views Vis Obgyn* 4, 102–109.

7. Alexander, J.L., Wilson, I.D., Teare, J., Marchesi, J.R., Nicholson, J.K., and Kinross, J.M. (2017). Gut microbiota modulation of chemotherapy efficacy and toxicity. *Nat. Rev. Gastroenterol. Hepatol.* *14*, 356–365. <https://doi.org/10.1038/nrgastro.2017.20>.
8. Ting, N.L., Lau, H.C., and Yu, J. (2022). Cancer pharmacomicrobiomics: targeting microbiota to optimise cancer therapy outcomes. *Gut* *71*, 1412–1425. <https://doi.org/10.1136/gutjnl-2021-326264>.
9. Iida, N., Dzutsev, A., Stewart, C.A., Smith, L., Bouladoux, N., Weingarten, R.A., Molina, D.A., Salcedo, R., Back, T., Cramer, S., et al. (2013). Commensal bacteria control cancer response to therapy by modulating the tumor microenvironment. *Science* *342*, 967–970. <https://doi.org/10.1126/science.1240527>.
10. Viaud, S., Saccheri, F., Mignot, G., Yamazaki, T., Daillere, R., Hannani, D., Enot, D.P., Pfirschke, C., Engblom, C., Pittet, M.J., et al. (2013). The intestinal microbiota modulates the anticancer immune effects of cyclophosphamide. *Science* *342*, 971–976. <https://doi.org/10.1126/science.1240537>.
11. Rottenberg, S., Disler, C., and Perego, P. (2021). The rediscovery of platinum-based cancer therapy. *Nat. Rev. Cancer* *21*, 37–50. <https://doi.org/10.1038/s41568-020-00308-y>.
12. Tintelnot, J., Xu, Y., Lesker, T.R., Schönlein, M., Konczalla, L., Giannou, A.D., Pelczar, P., Kyllies, D., Puelles, V.G., Bielecka, A.A., et al. (2023). Microbiota-derived 3-IAA influences chemotherapy efficacy in pancreatic cancer. *Nature* *615*, 168–174. <https://doi.org/10.1038/s41586-023-05728-y>.
13. Gupta, N., Ferreira, J., Hong, C.H.L., and Tan, K.S. (2020). *Lactobacillus reuteri* DSM 17938 and ATCC PTA 5289 ameliorates chemotherapy-induced oral mucositis. *Sci. Rep.* *10*, 16189. <https://doi.org/10.1038/s41598-020-73292-w>.
14. Wu, J., Zhuo, Y., Liu, Y., Chen, Y., Ning, Y., and Yao, J. (2021). Association between premature ovarian insufficiency and gut microbiota. *BMC Pregnancy Childbirth* *21*, 418. <https://doi.org/10.1186/s12884-021-03855-w>.
15. Li, P., Shuai, P., Shen, S., Zheng, H., Sun, P., Zhang, R., Lan, S., Lan, Z., Jayawardana, T., Yang, Y., et al. (2023). Perturbations in gut microbiota composition in patients with polycystic ovary syndrome: a systematic review and meta-analysis. *BMC Med.* *21*, 302. <https://doi.org/10.1186/s12916-023-02975-8>.
16. Qi, X., Yun, C., Sun, L., Xia, J., Wu, Q., Wang, Y., Wang, L., Zhang, Y., Liang, X., Wang, L., et al. (2019). Gut microbiota-bile acid-interleukin-22 axis orchestrates polycystic ovary syndrome. *Nat. Med.* *25*, 1225–1233. <https://doi.org/10.1038/s41591-019-0509-0>.
17. Li, A., Li, F., Song, W., Lei, Z.L., Sha, Q.Q., Liu, S.Y., Zhou, C.Y., Zhang, X., Li, X.Z., Schatten, H., et al. (2023). Gut microbiota-bile acid-vitamin D axis plays an important role in determining oocyte quality and embryonic development. *Clin. Transl. Med.* *13*, e1236. <https://doi.org/10.1002/ctm2.1236>.
18. Chen, X., Li, P., Liu, M., Zheng, H., He, Y., Chen, M.X., Tang, W., Yue, X., Huang, Y., Zhuang, L., et al. (2020). Gut dysbiosis induces the development of pre-eclampsia through bacterial translocation. *Gut* *69*, 513–522. <https://doi.org/10.1136/gutjnl-2019-319101>.
19. Dasari, S., and Bernard Tchounwou, P. (2014). Cisplatin in cancer therapy: Molecular mechanisms of action. *Eur. J. Pharmacol.* *740*, 364–378. <https://doi.org/10.1016/j.ejphar.2014.07.025>.
20. Spears, N., Lopes, F., Stefansdottir, A., Rossi, V., De Felici, M., Anderson, R.A., and Klinger, F.G. (2019). Ovarian damage from chemotherapy and current approaches to its protection. *Hum. Reprod. Update* *25*, 673–693. <https://doi.org/10.1093/humupd/dmz027>.
21. He, Y., Wang, Q., Li, X., Wang, G., Zhao, J., Zhang, H., and Chen, W. (2020). Lactic acid bacteria alleviate polycystic ovarian syndrome by regulating sex hormone related gut microbiota. *Food Funct.* *11*, 5192–5204. <https://doi.org/10.1039/c9fo02554a>.
22. Zhao, L., Xing, C., Sun, W., Hou, G., Yang, G., and Yuan, L. (2018). *Lactobacillus* supplementation prevents cisplatin-induced cardiotoxicity possibly by inflammation inhibition. *Cancer Chemother. Pharmacol.* *82*, 999–1008. <https://doi.org/10.1007/s00280-018-3691-8>.
23. Sharma, A., Rath, G.K., Chaudhary, S.P., Thakar, A., Mohanti, B.K., and Bahadur, S. (2012). *Lactobacillus brevis* CD2 lozenges reduce radiation- and chemotherapy-induced mucositis in patients with head and neck cancer: a randomized double-blind placebo-controlled study. *Eur. J. Cancer* *48*, 875–881. <https://doi.org/10.1016/j.ejca.2011.06.010>.
24. de Vos, W.M., Tilg, H., Van Hul, M., and Cani, P.D. (2022). Gut microbiome and health: mechanistic insights. *Gut* *71*, 1020–1032. <https://doi.org/10.1136/gutjnl-2021-326789>.
25. de Vargas, I., Macaskie, L.E., and Guibal, E. (2003). Biosorption of palladium and platinum by sulfate-reducing bacteria. *J. Chem. Technol. Biotechnol.* *79*, 49–56. <https://doi.org/10.1002/jctb.928>.
26. Lu, G., Zhang, Y., Ren, Y., Shi, J.S., Xu, Z.H., and Geng, Y. (2023). Diversity and Comparison of Intestinal *Desulfovibrio* in Patients with Liver Cirrhosis and Healthy People. *Microorganisms* *11*, 276. <https://doi.org/10.3390/microorganisms11020276>.
27. Rowley, J.E., Amargant, F., Zhou, L.T., Galligos, A., Simon, L.E., Pritchard, M.T., and Duncan, F.E. (2020). Low Molecular Weight Hyaluronan Induces an Inflammatory Response in Ovarian Stromal Cells and Impairs Gamete Development In Vitro. *Int. J. Mol. Sci.* *21*, 1036. <https://doi.org/10.3390/ijms21031036>.
28. Zhou, J., Jin, X., Sheng, Z., and Zhang, Z. (2021). miR-206 serves an important role in polycystic ovary syndrome through modulating ovarian granulosa cell proliferation and apoptosis. *Exp. Ther. Med.* *21*, 179. <https://doi.org/10.3892/etm.2021.9610>.
29. Sun, Q.Y., Ding, L.W., Johnson, K., Zhou, S., Tyner, J.W., Yang, H., Doan, N.B., Said, J.W., Xiao, J.F., Loh, X.Y., et al. (2019). SOX7 regulates MAPK/ERK-BIM mediated apoptosis in cancer cells. *Oncogene* *38*, 6196–6210. <https://doi.org/10.1038/s41388-019-0865-8>.
30. Wat, J.J., and Wat, M.J. (2014). Sox7 in vascular development: review, insights and potential mechanisms. *Int. J. Dev. Biol.* *58*, 1–8. <https://doi.org/10.1387/ijdb.130323mw>.
31. Costa, G., Mazan, A., Gandillet, A., Pearson, S., Lacaud, G., and Kouskoff, V. (2012). SOX7 regulates the expression of VE-cadherin in the haemogenic endothelium at the onset of haematopoietic development. *Development* *139*, 1587–1598. <https://doi.org/10.1242/dev.071282>.
32. Hafezi, S., and Rahmani, M. (2021). Targeting BCL-2 in Cancer: Advances, Challenges, and Perspectives. *Cancers* *13*, 1292. <https://doi.org/10.3390/cancers13061292>.
33. Takash, W., Cañizares, J., Bonneaud, N., Poulat, F., Mattéi, M.G., Jay, P., and Berta, P. (2001). SOX7 transcription factor: sequence, chromosomal localisation, expression, transactivation and interference with Wnt signalling. *Nucleic Acids Res.* *29*, 4274–4283. <https://doi.org/10.1093/nar/29.21.4274>.
34. Miao, Y., Cui, Z., Gao, Q., Rui, R., and Xiong, B. (2020). Nicotinamide Mononucleotide Supplementation Reverses the Declining Quality of Maternally Aged Oocytes. *Cell Rep.* *32*, 107987. <https://doi.org/10.1016/j.celrep.2020.107987>.
35. European Society for Human, R., Embryology Guideline Group on, P.O.I., Webber, L., Davies, M., Anderson, R., Bartlett, J., Braat, D., Cartwright, B., Cifkova, R., de Muinck Keizer-Schrama, S., et al. (2016). ESHRE Guideline: management of women with premature ovarian insufficiency. *Hum. Reprod.* *31*, 926–937. <https://doi.org/10.1093/humrep/dew027>.
36. Anderson, R.A., Brewster, D.H., Wood, R., Nowell, S., Fischbacher, C., Kelsey, T.W., and Wallace, W.H.B. (2018). The impact of cancer on subsequent chance of pregnancy: a population-based analysis. *Hum. Reprod.* *33*, 1281–1290. <https://doi.org/10.1093/humrep/dey216>.
37. Hsiao, Y.P., Chen, H.L., Tsai, J.N., Lin, M.Y., Liao, J.W., Wei, M.S., Ko, J.L., and Ou, C.C. (2021). Administration of *Lactobacillus reuteri* Combined with *Clostridium butyricum* Attenuates Cisplatin-Induced Renal Damage by Gut Microbiota Reconstitution, Increasing Butyric Acid

- Production, and Suppressing Renal Inflammation. *Nutrients* 13, 2792. <https://doi.org/10.3390/nu13082792>.
38. Lee, T.H., Park, D., Kim, Y.J., Lee, I., Kim, S., Oh, C.T., Kim, J.Y., Yang, J., and Jo, S.K. (2020). Lactobacillus salivarius BP121 prevents cisplatin-induced acute kidney injury by inhibition of uremic toxins such as indoxyl sulfate and p-cresol sulfate via alleviating dysbiosis. *Int. J. Mol. Med.* 45, 1130–1140. <https://doi.org/10.3892/ijmm.2020.4495>.
  39. Wu, Y., Wu, J., Lin, Z., Wang, Q., Li, Y., Wang, A., Shan, X., and Liu, J. (2021). Administration of a Probiotic Mixture Ameliorates Cisplatin-Induced Mucositis and Pica by Regulating 5-HT in Rats. *J. Immunol. Res.* 2021, 9321196. <https://doi.org/10.1155/2021/9321196>.
  40. Gui, Q.F., Lu, H.F., Zhang, C.X., Xu, Z.R., and Yang, Y.H. (2015). Well-balanced commensal microbiota contributes to anti-cancer response in a lung cancer mouse model. *Genet. Mol. Res.* 14, 5642–5651. <https://doi.org/10.4238/2015.May.25.16>.
  41. Widmeier, E., Yu, S., Nag, A., Chung, Y.W., Nakayama, M., Fernández-Del-Río, L., Hugo, H., Schapiro, D., Buerger, F., Choi, W.I., et al. (2020). ADCK4 Deficiency Destabilizes the Coenzyme Q Complex, Which Is Rescued by 2,4-Dihydroxybenzoic Acid Treatment. *J. Am. Soc. Nephrol.* 31, 1191–1211. <https://doi.org/10.1681/asn.2019070756>.
  42. Widmeier, E., Airik, M., Hugo, H., Schapiro, D., Wedel, J., Ghosh, C.C., Nakayama, M., Schneider, R., Awad, A.M., Nag, A., et al. (2019). Treatment with 2,4-Dihydroxybenzoic Acid Prevents FSGS Progression and Renal Fibrosis in Podocyte-Specific Coq6 Knockout Mice. *J. Am. Soc. Nephrol.* 30, 393–405. <https://doi.org/10.1681/asn.2018060625>.
  43. Hidalgo-Gutiérrez, A., Barriocanal-Casado, E., Bakkali, M., Diaz-Casado, M.E., Sanchez-Maldonado, L., Romero, M., Sayed, R.K., Prehn, C., Escames, G., Duarte, J., et al. (2019). beta-RA reduces DMQ/CoQ ratio and rescues the encephalopathic phenotype in Coq9(R239X) mice. *EMBO Mol. Med.* 11, e9466. <https://doi.org/10.15252/emmm.201809466>.
  44. Visser, J.A., Schipper, I., Laven, J.S., and Themmen, A.P. (2012). Anti-Müllerian hormone: an ovarian reserve marker in primary ovarian insufficiency. *Nat. Rev. Endocrinol.* 8, 331–341. <https://doi.org/10.1038/nrendo.2011.224>.
  45. Richani, D., Dunning, K.R., Thompson, J.G., and Gilchrist, R.B. (2021). Metabolic co-dependence of the oocyte and cumulus cells: essential role in determining oocyte developmental competence. *Hum. Reprod. Update* 27, 27–47. <https://doi.org/10.1093/humupd/dmaa043>.
  46. Yuksel, A., Bildik, G., Senbabaoglu, F., Akin, N., Arvas, M., Unal, F., Kilic, Y., Karanfil, I., Eryilmaz, B., Yilmaz, P., et al. (2015). The magnitude of gonadotoxicity of chemotherapy drugs on ovarian follicles and granulosa cells varies depending upon the category of the drugs and the type of granulosa cells. *Hum. Reprod.* 30, 2926–2935. <https://doi.org/10.1093/humrep/dev256>.
  47. De Vos, M., Smits, J., and Woodruff, T.K. (2014). Fertility preservation in women with cancer. *Lancet (London, England)* 384, 1302–1310. [https://doi.org/10.1016/s0140-6736\(14\)60834-5](https://doi.org/10.1016/s0140-6736(14)60834-5).
  48. Matsuda, F., Inoue, N., Manabe, N., and Ohkura, S. (2012). Follicular growth and atresia in mammalian ovaries: regulation by survival and death of granulosa cells. *J. Reprod. Dev.* 58, 44–50. <https://doi.org/10.1262/jrd.2011-012>.
  49. Yang, F., Chen, Y., Liu, Q., Dai, S., and Zeng, S. (2020). Dynamics and Regulations of BimEL Ser65 and Thr112 Phosphorylation in Porcine Granulosa Cells during Follicular Atresia. *Cells* 9, 402. <https://doi.org/10.3390/cells9020402>.
  50. Griffiths, M.J., Winship, A.L., and Hutt, K.J. (2020). Do cancer therapies damage the uterus and compromise fertility? *Hum. Reprod. Update* 26, 161–173. <https://doi.org/10.1093/humupd/dmz041>.
  51. Clift, D., and Schuh, M. (2013). Restarting life: fertilization and the transition from meiosis to mitosis. *Nat. Rev. Mol. Cell Biol.* 14, 549–562. <https://doi.org/10.1038/nrm3643>.
  52. Hao, X., Anastacio, A., Liu, K., and Rodriguez-Wallberg, K.A. (2019). Ovarian Follicle Depletion Induced by Chemotherapy and the Investigational Stages of Potential Fertility-Protective Treatments-A Review. *Int. J. Mol. Sci.* 20, 4720. <https://doi.org/10.3390/ijms20194720>.
  53. Qin, X., Zhao, Y., Zhang, T., Yin, C., Qiao, J., Guo, W., and Lu, B. (2022). TrkB agonist antibody ameliorates fertility deficits in aged and cyclophosphamide-induced premature ovarian failure model mice. *Nat. Commun.* 13, 914. <https://doi.org/10.1038/s41467-022-28611-2>.
  54. Furlanetto, J., Marmé, F., Seiler, S., Thode, C., Untch, M., Schmatloch, S., Schneeweiss, A., Bassy, M., Fasching, P.A., Strik, D., et al. (2021). Chemotherapy-induced ovarian failure in young women with early breast cancer: Prospective analysis of four randomised neoadjuvant/adjunct breast cancer trials. *Eur. J. Cancer* 152, 193–203. <https://doi.org/10.1016/j.ejca.2021.04.038>.
  55. Liu, M., Li, W., Zhou, X., Zhou, M., Zhang, W., Liu, Q., Zhang, A., and Xu, B. (2022). Cell-Free Fat Extract Improves Ovarian Function and Fertility in Mice With Advanced Age. *Front. Endocrinol.* 13, 912648. <https://doi.org/10.3389/fendo.2022.912648>.
  56. Bolyen, E., Rideout, J.R., Dillon, M.R., Bokulich, N.A., Abnet, C.C., Al-Ghalith, G.A., Alexander, H., Alm, E.J., Arumugam, M., Asnicar, F., et al. (2019). Reproducible, interactive, scalable and extensible microbiome data science using QIIME 2. *Nat. Biotechnol.* 37, 852–857. <https://doi.org/10.1038/s41587-019-0209-9>.
  57. Callahan, B.J., McMurdie, P.J., Rosen, M.J., Han, A.W., Johnson, A.J., and Holmes, S.P. (2016). DADA2: High-resolution sample inference from Illumina amplicon data. *Nat. Methods* 13, 581–583. <https://doi.org/10.1038/nmeth.3869>.
  58. DeSantis, T.Z., Hugenholtz, P., Larsen, N., Rojas, M., Brodie, E.L., Keller, K., Huber, T., Dalevi, D., Hu, P., and Andersen, G.L. (2006). Greengenes, a chimera-checked 16S rRNA gene database and workbench compatible with ARB. *Appl. Environ. Microbiol.* 72, 5069–5072. <https://doi.org/10.1128/aem.03006-05>.
  59. Beghini, F., McIver, L.J., Blanco-Míguez, A., Dubois, L., Asnicar, F., Maharjan, S., Mailyan, A., Manghi, P., Scholz, M., Thomas, A.M., et al. (2021). Integrating taxonomic, functional, and strain-level profiling of diverse microbial communities with bioBakery 3. *Elife* 10, e65088. <https://doi.org/10.7554/eLife.65088>.
  60. Segata, N., Izard, J., Waldron, L., Gevers, D., Miropolsky, L., Garrett, W.S., and Huttenhower, C. (2011). Metagenomic biomarker discovery and explanation. *Genome Biol.* 12, R60. <https://doi.org/10.1186/gb-2011-12-6-r60>.
  61. Zheng, H., Mai, F., Zhang, S., Lan, Z., Wang, Z., Lan, S., Zhang, R., Liang, D., Chen, G., Chen, X., and Feng, Y. (2024). In silico method to maximise the biological potential of understudied metabolomic biomarkers: a study in pre-eclampsia. *Gut* 73, 383–385. <https://doi.org/10.1136/gutjnl-2022-329312>.
  62. Bernal, A.B., Vickers, M.H., Hampton, M.B., Poynton, R.A., and Sloboda, D.M. (2010). Maternal undernutrition significantly impacts ovarian follicle number and increases ovarian oxidative stress in adult rat offspring. *PLoS One* 5, e15558. <https://doi.org/10.1371/journal.pone.0015558>.
  63. Borgeest, C., Symonds, D., Mayer, L.P., Hoyer, P.B., and Flaws, J.A. (2002). Methoxychlor may cause ovarian follicular atresia and proliferation of the ovarian epithelium in the mouse. *Toxicol. Sci.* 68, 473–478. <https://doi.org/10.1093/toxsci/68.2.473>.
  64. Sundqvist, A., Morikawa, M., Ren, J., Vasilaki, E., Kawasaki, N., Kobayashi, M., Koinuma, D., Aburatani, H., Miyazono, K., Heldin, C.H., et al. (2018). JUNB governs a feed-forward network of TGFβ signaling that aggravates breast cancer invasion. *Nucleic Acids Res.* 46, 1180–1195. <https://doi.org/10.1093/nar/gkx1190>.
  65. Chen, S., Zhou, Y., Chen, Y., and Gu, J. (2018). fastp: an ultra-fast all-in-one FASTQ preprocessor. *Bioinformatics* 34, i884–i890. <https://doi.org/10.1093/bioinformatics/bty560>.
  66. Zhang, Y., Liu, T., Meyer, C.A., Eeckhoute, J., Johnson, D.S., Bernstein, B.E., Nussbaum, C., Myers, R.M., Brown, M., Li, W., and Liu, X.S. (2008). Model-based analysis of ChIP-Seq (MACS). *Genome Biol.* 9, R137. <https://doi.org/10.1186/gb-2008-9-9-r137>.

## STAR★METHODS

### KEY RESOURCES TABLE

REAGENT or RESOURCE	SOURCE	IDENTIFIER
<b>Antibodies</b>		
Anti-SOX7 Antibody	R&D	Cat# AF2766; RRID: AB_2196241
Anti-BAX Antibody	Cell Signaling	Cat# 2774; RRID: AB_490806
Anti-BCL-2 Antibody	Cell Signaling	Cat# 26295; RRID: AB_2798920
Anti-GAPDH Antibody	Abcam	Cat# ab8245; RRID: AB_2107448
HRP-conjugated anti-rabbit Antibody	Cell Signaling	Cat# 7074P2; RRID: AB_2099233
Donkey anti-goat Antibody	Life technologies	Cat# A-11055; RRID: AB_2534102
<b>Bacterial and virus strains</b>		
<i>Limosilactobacillus reuteri</i> DSM 17938	CGMCC	Cat# 1.12733
<b>Chemicals, peptides, and recombinant proteins</b>		
β-RA	Macklin	Cat# D806751
Cisplatin	Macklin	Cat# D807330
Vancomycin	Macklin	Cat# V871983
Neomycin sulfate	Macklin	Cat# N6063
Metronidazole	Macklin	Cat# M813525
Ampicillin	Macklin	Cat# A830931
Paraformaldehyde	Macklin	Cat# P885233
Glutaraldehyde	Macklin	Cat# G810415
LC/MS -grade methanol	Sigma	Cat# 1.06035
Formic acid	Macklin	Cat# F809712
Acetonitrile	Sigma	Cat# CN34891
Hyaluronidase	Sigma	Cat# H4272
Formaldehyde	Sigma	Cat# 252549
Glycerine	Macklin	Cat# 810575
Sodium bicarbonate	Macklin	Cat# S818079
Sodium diethyldithiocarbamate	Macklin	Cat# S817628
Pregnant mare serum gonadotropin	Ningbo Second Hormone Factory	Cat# GN024
Human chorionic gonadotropin	Ningbo Second Hormone Factory	Cat# GN026
Hyaluronidase	Sigma	Cat# H1115000
de Man, Rogosa and Sharpe broth	Hopebio	Cat# HB0384-5
DMEM	Gibco	Cat# C11995500BT
DMEM/F12(1:1) medium	Gibco	Cat# C11330500BT
0.25%Trysin-EDTA	Gibco	Cat# 25200072
Bovine Serum Albumin	Sigma	Cat# V900933
Opti-MEN	Gibco	Cat# 31985070
TRIzol reagent	Invitrogen	Cat# 15596018
RIPA lysis buffer	Thermo Scientific	Cat# 89901
Protease and phosphatase inhibitors	Thermo Scientific	Cat# 78442
HTF medium	Nanjing Aibei Biotechnology	Cat# M1130
KOSM medium	Nanjing Aibei Biotechnology	Cat# M1430
Light oil (neat)	Sigma	Cat# M840
<b>Deposited data</b>		
ChIP-Seq	This paper	CNSA: CNP0002833
16S rRNA sequencing	This paper	CNSA: CNP0002837
Metagenome	This paper	CNSA: CNP0002838

(Continued on next page)

REAGENT or RESOURCE	SOURCE	IDENTIFIER
<b>Continued</b>		
<b>Critical commercial assays</b>		
TUNEL Assay Kit	Keygenbio	Cat# KGA703
Mouse FSH ELISA kits	MEIMIAN	Cat# MM-0566M1
Mouse E <sub>2</sub> ELISA kit	MEIMIAN	Cat# MM-45654 M1
Human FSH ELISA kit	Bioswamp	Cat# HM10662
Human E2 ELISA kit	Bioswamp	Cat# HM10669
Human AMH ELISA kit	Bioswamp	Cat# HM10844
Lipofectamine 3000 Reagent	Thermo Fisher	Cat# L3000015
CCK-8 assay	Beyotime	Cat# C0038
Annexin V-FITC/PI apoptosis kit	MULTISCIENCES	Cat# 70-AP101-100
Reverse Transcription Kit	Toyobo	Cat# KMM-101
SYBR qPCR Mix	Toyobo	Cat# QPX-201
BCA protein assay kit	Thermo	Cat# 23227
Nuclear and Cytoplasmic Extraction Kit	Beyotime	Cat# P0028
Plus Enzymatic Chromatin IP Kit	Cell Signaling	Cat# 9005S
Dual-luciferase reporter gene system	Promega	Cat# PR-E1910
<b>Experimental models: Organisms/strains</b>		
C56Bl/6J	SiPeiFu	N/A
<b>Experimental models: Cell lines</b>		
Human granulosa cell line (KGNs)	ATCC	Cat# CL-0603
Mouse ovarian cancer cell line (ID8)	BNCC	Cat# BNCC339488
Mouse Lewis lung carcinoma cell line	BNCC	Cat# BNCC338433
<b>Oligonucleotides</b>		
List of primers	Table S4	N/A
<b>Software and algorithms</b>		
R	R Core Team	<a href="https://www.r-project.org/">https://www.r-project.org/</a>
GraphPad Prism 7	GraphPad Software	<a href="https://www.graphpad.com/">https://www.graphpad.com/</a>
Python	Python Software Foundation	<a href="https://www.python.org">https://www.python.org</a>

## RESOURCE AVAILABILITY

### Lead contact

Further information and requests for resources should be directed to and will be fulfilled by the lead contact, Xia Chen ([chenx\\_fsyy@163.com](mailto:chenx_fsyy@163.com)).

### Materials availability

This study did not generate new reagents.

### Data and code availability

- The 16S rRNA-seq, ChIP-Seq and metagenome data have been deposited in the Chinese National Gene Bank Nucleotide Sequence Archive (<https://db.cngb.org/cnsa/>, Accession numbers: CNP0002833, CNP0002837, CNP0002838 for 16S rRNA-seq, ChIP-seq, and metagenome data, respectively). Accession numbers are also listed in the [key resources table](#). Microscopy data reported in this paper will be shared by the [lead contact](#) upon request.
- This paper does not report the original code.
- Any additional information required to reanalyze the data reported in this paper is available from the [lead contact](#) upon request.

## EXPERIMENTAL MODEL AND SUBJECT DETAILS

### Patients and clinical specimens

We recruited the cohort of CIPOI patients from First People's Hospital of Foshan in 2021. Twenty-one patients enrolled in the periodical follow-up six months after the last cisplatin-base chemotherapy treatment. Enrolled patients who were diagnosed as

POI based on the criteria: amenorrhea for at least four months and the postmenopausal level of FSH (12.4 IU/L) and estradiol (<52.2 ng/L).<sup>54</sup> Eligible patients had taken no oestrogens, antioestrogens, selective oestrogen-receptor modulators, aromatase inhibitors or hormonal contraceptives within six months before enrollment. Patients who were over the age of 40, actually diagnosed with POI before chemotherapy, had undergone bilateral ovariectomy and radiotherapy, with family history of POI were excluded. Eighteen healthy controls were age-match females who had regular menstrual cycles, normal levels of FSH and estradiol from the general community. None of the individuals had received antibiotics or probiotics during the previous two months or had undergone bilateral ovariectomy and radiotherapy. None of the individual consumed fermented foods frequently. This study was approved by the ethics committee of First People's Hospital of Foshan (approval no.: FSYYY-EC-SOP-2021-047). All individuals provided written consent before donating stool and blood samples. The clinical characteristics of donors were summarized in [Table S3](#).

### Murine studies

Female C57/BL6 mice (8 weeks, weight 18-20g) were purchased from SiPeiFu Biotechnology (Beijing, China) and housed in specific pathogen-free (SPF) conditions with temperature control ( $22 \pm 1^\circ\text{C}$ ) and humidity control ( $60 \pm 10\%$ ) on a 12 h light/12 h dark cycle schedule with free access to food and water. Germ-free female mice were provided by Cyagen Biosciences Inc. (Suzhou, China) and housed under germ-free conditions. All experimental procedures were performed under the National Institutes of Health guidelines and were approved by the local Animal Care and Use Committee of the First People's Hospital of Foshan (Approval No.C202103-30).

For the cisplatin-induced POI (*Cis*-POI) model, mice were weighed and injected intraperitoneally with 1.5 mg/kg cisplatin (Macklin, Shanghai, China) daily for 7 consecutive days. For the ID8 ovarian cancer (OvCa) and Lewis lung carcinoma (LLC) model,  $5 \times 10^6$  cells ID8 cells or  $2 \times 10^5$  LLC cells were harvested in the logarithmic growth phase and subcutaneously injected into mice. Approximately 14 days post-implantation (tumors 100-150mm<sup>3</sup>), mice were randomized and assigned to groups and treated with cisplatin, *L. reuteri* or  $\beta$ -RA.

FMT was performed as previously described.<sup>18</sup> Feces from donor mice were collected and resuspended in PBS at 0.125 g/mL. Mice were randomly divided into two groups after ABX (vancomycin, 100 mg/kg; neomycin sulfate, metronidazole and ampicillin, 200 mg/kg) treatment and 0.20 mL fecal supernatants were administered to the mice by gavage once daily for 3 days prior to *Cis*-POI modeling, and twice per week thereafter. For administration of *L. reuteri*, *L. reuteri* was orally gavaged at a dose of  $1 \times 10^9$  colony-forming units (CFU) per 0.2 mL suspended in PBS for 3 days prior to *Cis*-POI modeling. Subsequently, the mice were administered *L. reuteri* via oral gavage on days 1, 2, 3, 6, and 7 of modeling. For  $\beta$ -RA administration, mice were fed 600  $\mu\text{M}$   $\beta$ -RA in drinking water 3 days before cisplatin administration and throughout the modeling period. To knock down *Sox7* in mice, siRNA against mouse *Sox7* was synthesized and purchased from Guangzhou RiboBio Co., Ltd. The sequence CCACGGCCACGTATTACAA was used for targeted silencing of *Sox7*, and Si-NC (siN0000001-1-5, Guangzhou RiboBio Co., Ltd) administration was used as control. Then, siRNA (2 mg/kg) was injected into the mice via the tail vein 48 h before the cisplatin intervention. On the second day of *Cis*-POI modeling, the same dose of siRNA was administered. The animals were sacrificed to collect specimens after seven days of modeling.

To assess the efficiency of  $\beta$ -RA involved in the improvement of fertility, reproductive tests were conducted. Two weeks after the last treatment of cisplatin, female mice from *Cis*-POI groups and *Cis*-POI+ $\beta$ -RA were mated with sexually mature male mice in a 2:1 ratio for 10 days and the fertility information was recorded. Following this, male and female mice separated for 18 days to confirm the final pregnancy status. During the process, the interval time (the time from mating to birth) and the number of offspring were recorded.<sup>55</sup> Fifteen mice per group were included at the first round of reproductive test. Two mice from the *Cis*-POI group and one from the *Cis*-POI+ $\beta$ -RA group died during mating due to feebleness. One *Cis*-POI mouse died during delivery due to dystocia. To assess the recovery of reproductive ability after damage of cisplatin, we performed the second round of reproductive test. After the first round of delivery, the mice in the postnatal period as well as the mice who fail to conceive were reintroduced to the males for the second round of reproductive assay. One mouse from the *Cis*-POI+ $\beta$ -RA group delivered and ate the pups, which led to the loss of fetal data from this mouse.

### Bacterial strains and growth condition

*L. reuteri* DSM 17938 was obtained from the China General Microbiological Culture Collection Center and confirmed by 16S rRNA sequencing. The bacteria were initially cultured and maintained under anaerobic conditions on MRS media (Macklin, Shanghai, China) at 37°C. To prepare bacteria for oral treatment, *L. reuteri* was cultured under anaerobic conditions at 37°C on fresh MRS, grown until log phase (OD<sub>600</sub> = 0.8), spun down, washed with sterile PBS, and stored at  $-80^\circ\text{C}$ .

### Cell lines

The human granulosa cell line (KGN) was purchased from the American Type Culture Collection (Manassas, VA, USA), the murine ovarian surface epithelial cancer cell lines (ID8) and the murine Lewis lung cancer cell lines (LLC) were purchased from the BeNa Culture Collection (Beijing, China). KGN cells were cultured in DMEM/F12 supplemented with 10% fetal bovine serum (FBS). ID8 and LLC cells were cultured in DMEM supplemented with 10% FBS. The cells were maintained at 37°C with 5% CO<sub>2</sub>, and the medium was changed every other day until the cells reached 90% confluence.

## METHOD DETAILS

### Sequencing and analysis

For 16S rRNA sequencing, human fecal samples were sequenced using 250 bp paired end reads on the Illumina NovaSeq 6000 platform. We used the standardized pipeline in QIIME2 to process and analyze 16S rRNA sequencing data.<sup>56</sup> The DADA2 algorithm<sup>57</sup> and the Greengenes v13\_8 database<sup>58</sup> were employed to generate amplicon sequence variants (ASVs) and assign taxonomy, respectively.

For shotgun metagenome sequencing, human fecal samples were sequenced using 150 bp paired end reads on the Illumina NovaSeq 6000 platform. Quality control of the reads was performed using Bowtie2 (v2.4.1) based on the human genome reference (hg38) to filter adapter contamination and low-quality reads from the raw sequencing reads. The remaining reads were subjected to microbial taxon and gene identification using Kraken2<sup>58</sup> and HuMAN3.<sup>59</sup> Alpha and beta diversities were calculated using QIIME2. ORA was employed to identify significant microbial pathways associated with the differentially expressed microbial genes predicted by HuMAN3 from shotgun metagenome data. Linear discriminant analysis effect size (LEfSe) was performed to determine the different gut microbial features between the groups.<sup>60</sup>

LC-MS/MS analyses were performed using a UHPLC system (Vanquish, Thermo Fisher Scientific) with a UPLC BEH (2.1 mm × 100 mm, 1.7 μm) Amide column coupled to Q Exactive HFX mass spectrometer (Orbitrap MS, Thermo). The mobile phase comprised 25 mM ammonium acetate, 25 mM ammonia hydroxide in water (pH = 9.75), and acetonitrile. The auto-sampler temperature was 4°C and the injection volume was 3 μL. The QE HFX mass spectrometer was used because of its ability to acquire MS/MS spectra in information-dependent acquisition (IDA) mode in the control of the acquisition software (Xcalibur, Thermo). In this mode, the acquisition software continuously evaluated the full-scan MS spectrum. The ESI source conditions were set as follows: sheath gas flow rate, 30 Arb; Aux gas flow rate, 25 Arb; capillary temperature, 350°C; full MS resolution, 60000; MS/MS resolution, 7500; collision energy, 10/30/60 in NCE mode; and spray voltage, 3.6 (positive) or −3.2 kV (negative). To better analyze the data, we conducted data management procedures on the original data. This mainly included the following steps: (1) filtering a single peak to remove noise, the deviation value filtered based on the relative standard deviation (RSD, namely coefficient of variation, CV), filtering a single peak, or only the peak area data with one group of null values not over 50% or all groups of null values not over 50% were retained; (2) simulating missing values in raw data (missing value recording); the numerical simulation method was filled by the minimum half method; data normalization and internal standard (IS) were used for normalization. The data analyses were performed using an established protocol described in our previous study.<sup>61</sup> PCA was performed using the R package psych (v2.1.6), and a volcano plot was generated using the R package Enhanced Volcano (v1.10.0). A combination of in-house and online databases (<https://hmdb.ca/>) was obtained from Magigene (Guangzhou, China).

### Histological analysis and follicular count

The ovaries were fixed in 4% paraformaldehyde overnight and embedded in paraffin. Serial sections 3 μm thick were stained with H&E. Ovarian follicles were counted according to the methods described in a previous study.<sup>62</sup> Briefly, every fifth section was observed under a light microscope. To avoid repeated counting, only follicles with visible oocytes were included. Follicles were classified as in previous experiments.<sup>63</sup> Primordial follicles have one layer of flattened granulosa cells surrounding the oocyte; primary follicles are those where the oocyte is encircled by a single layer of columnar granulosa cells; secondary follicles comprise the oocyte surrounded by several layers of granulosa cells, with no antrum; in an antral follicle, the oocyte has multiple layers of granulosa cells and a follicular cavity; in an atretic follicle, the oocyte has entered a degenerative process without ovulation.

### TUNEL staining

TUNEL staining was used to evaluate ovarian apoptosis, according to the manufacturer's instructions. Paraffin-embedded ovarian tissue sections were deparaffinized in xylene and rehydrated in decreasing concentrations of ethanol. The sections were permeabilized with 10 μg/mL proteinase K for 8 min. The sections were then washed and incubated with the labeling cocktail for 1 h at 37°C. All antral follicles in each group were examined. TUNEL-positive cells were stained red, and nuclei were stained with DAPI (blue). TUNEL-positive granulosa cells and total granulosa cells in the antral follicles were counted. The percentage of TUNEL-positive granulosa cells was determined in the antral follicles.

### Transmission electron microscopy (TEM)

To determine the ultrastructure of antral follicles using TEM, the ovaries were removed, fixed in 2.5% glutaraldehyde overnight at 4°C, and washed three times with phosphate-buffered saline. Subsequently, the samples were stained with uranyl acetate for 30 min, dehydrated using serial concentrations of ethanol, and embedded in a resin mixture. Sections were observed under a transmission electron microscope (Hitachi H-7500, Japan).

### ELISA

Serum hormone levels were measured by ELISA using commercially available ELISA assays. Mouse FSH kit, mouse E2 kit, human FSH kit, human E2 kit and human AMH kit were used. Briefly, standard antibody protein and serum samples in suitable dilutions were added to the wells and incubated for 1 h. The plates were incubated with HRP-labelled secondary antibodies for 30 min. The stopping

solution was added to each well to terminate the reaction. Finally, the absorbance at 450 nm was measured using a microplate reader (BioTek, Winooski, USA). Data were analyzed using CurveExpert version 1.4 program (Hyams D.G., Starkville, MS, USA).

### **In vivo pharmacokinetic study**

Eight-week-old female C57/BL6 mice with weights of 18–20g were categorized in different groups and treated with *L.reuteri* and  $\beta$ -RA. Mice in the *L.reuteri*- and  $\beta$ -RA-treated group were administered with  $1 \times 10^9$  CFU *L.reuteri* or 600mM  $\beta$ -RA for 3 consecutive days prior to cisplatin treatment. 1.5 mg/kg cisplatin was injected intraperitoneally. After administration of cisplatin into mice, blood samples were serially collected at 0, 15, 30, 60 min, 24, 48 and 72h, and kept in heparinized tubes. Urine samples were collected at 24, 48 and 72h. The levels of cisplatin in both plasma and urine were determined by high-performance liquid chromatography analysis.

### **Liquid chromatography/mass spectrometry**

The serum, feces, cecum, and bacterial solutions were precipitated using liquid chromatography/mass spectrometry-grade methanol. The concentration of  $\beta$ -RA in the supernatant of each sample was measured by UPLC (Agilent) with column,  $3.0 \times 0.25$  mm  $\times$   $0.25$   $\mu$ m (TG WAX). Mobile phase A was 0.1% formic acid and mobile phase B was acetonitrile. The gradient elution was conducted as follows: A 10% and B 90%;  $100^\circ\text{C}$  for 2 min,  $20^\circ\text{C}$  for 1 min,  $200^\circ\text{C}$  for 2 min. The flow rate was 1 mL/min. Mass spectral fragments  $m/z = 105$  were recorded. Serum and urine samples collected to detect the level of cisplatin were added with 0.5% sodium bicarbonate and 5% sodium diethyldithiocarbamate. Mix well and incubate at  $37^\circ\text{C}$  for 30 min. The solution was extracted with chloroform and centrifuged at  $15000g$  for 15min. 1mL supernatant was vacuum drying and reconstituted in methanol. A Total volume of 50 $\mu$ L sample was injected into a Hypersil ODS2 (250 mm  $\times$  46 mm,  $5\mu$ m) column (Thermo Scientific, MA, USA). For the detection of cisplatin, the mobile phase was methanol and pure water at a volume ratio of 80:20. The flow rate was 1 mL/min. Mass spectral fragments  $m/z = 105$  were recorded. The injection volume was 10 $\mu$ L and the UV detection wavelength was 254nm.

### **Superovulation, oocytes collection and granulosa cell isolation**

The number of ovulated oocytes morphologically normal or abnormal was recorded. Mice were super ovulated via a single intraperitoneal injection of 0.4IU/kg pregnant mare serum gonadotropin (PMSG), followed by injection of human chorionic gonadotropin (HCG) 48h later. The cumulus-oocyte complexes (COC) were collected from the ampulla portion of the oviduct at 14–16h after HCG injection. After treatment of 1 mg/mL hyaluronidase, the oocytes were removed by mouth pipetting to be observed and counted by light microscopy; the remaining cells were predominantly granulosa cells. Granulosa cells were collected in 1.5 mL microcentrifuge tubes, washed with PBS twice and centrifuged. One milliliter TRIzol reagent was added for total RNA extraction and transcriptome resequencing.

### **In vitro fertilization and embryo culture**

Caudae epididymis from 12-week-old male mice were lanced in a dish of HTF medium under mineral oil to release sperm, followed by being capacitated for 1h ( $37^\circ\text{C}$ , 5%  $\text{CO}_2$ ). COC were collected from 14 to 16h HCG injection and inseminated with capacitated spermatozoa at  $1 \times 10^6$  cells/ml. Inseminated oocytes were then thoroughly washed to remove adhered spermatozoa and cumulus cells by repeating pipetting.

The fertilized eggs were cultured in KOSM (potassium simplex optimization medium) under mineral oil at  $37^\circ\text{C}$  in a 5%  $\text{CO}_2$  atmosphere for up to 4 days (Day 0 of insemination). The presence of two pronuclei was scored as successful fertilization. The number of oocytes that develop to the 2-cell and morula embryo stages was recorded respectively.

### **Transcriptome resequencing and analysis**

Total RNA was extracted from GCs using TRIzol; RNA-seq was performed by Novogene (Beijing, China). Transcript-level abundance data were pre-processed using R/tximport and summarized at the gene level before further analysis. Reads were mapped to the mouse reference genome (<https://www.gnmpedia.org/trust/>) and the genes were ranked based on  $\log_2$ FoldChange. Heatmaps of differentially expressed genes (DGEs) were created with the R package ComplexHeatmap. A volcano plot of DEGs was generated using the following R packages: ggthemes (<https://cran.r-project.org/web/packages/ggpubr/index.html>) and ggpub (<https://www.rdocumentation.org/packages/ggpubr>). Gene ontology (GO) analyses were performed using the R package “clusterProfiler” (<https://bioconductor.org/packages/clusterProfiler/>, version 3.14.3).

### **Cell stimulation and transfections**

KGN cells were plated at  $0.5 \times 10^5$  cells in DMEM/F12 supplemented with 10% FBS and subsequently treated for 20 h with 10  $\mu$ M cisplatin. 50  $\mu$ M  $\beta$ -RA was added to the cells 6 h before cisplatin stimulation. siRNA with the sequence CGACCAGTATTTGAACACT was used for targeted silencing of Sox7 in KGN cells, and Si-NC (siN0000001-1-5, Guangzhou RiboBio Co., Ltd) was used as a control. siRNA transfection was performed in KGN cells using RNAiMAX transfection reagent, according to the manufacturer’s instructions. The efficiency of gene silencing was determined at 36 h after transfection using western blotting. Plasmid transfection was performed using Lipofectamine 3000 (Thermo Fisher Scientific). KGN cells were transfected with plasmids for 36 h according to the manufacturer’s instructions (1  $\mu$ g DNA, 1:2.5 DNA/Lipo w/w ratio).

## Cell proliferation assay

Cell proliferation was measured using a cell counting Kit-8 (CCK-8) assay. KGN cells in the exponential growth phase were seeded in 96-well plates. Ten microliters of CCK-8 solution were added following various treatments. Absorbance was measured at 450 nm using a microplate reader after incubation at 37°C for 1.5 h.

## Cell apoptosis

Apoptosis was detected using an Annexin V-FITC/PI apoptosis kit and TUNEL staining. KGN cells in the exponential growth phase were seeded in 6-well plates. After various treatments, the apoptosis assay was performed after the treatments, according to the manufacturer's instructions. Briefly, the cells were collected from the plates and washed twice with ice-cold PBS. Approximately  $10^5$  cells were suspended in 1 mL of binding buffer. Cells were stained with 5  $\mu$ L Annexin and 10  $\mu$ L PI for 10 min in the dark and analyzed using flow cytometry. (For V-FITC, Ex = 488 nm, Em = 530 nm; For PI, Ex = 535 nm, Em = 615 nm). The TUNEL kit was used to stain apoptotic cells. Cell staining was performed as previously described. TUNEL-positive cells in at least five random fields of each sample were counted under a fluorescence microscope (Olympus Japan, Tokyo, Japan).

## Quantitative reverse-transcription PCR

RNA was isolated from KGN cells and mice ovaries using TRIzol reagent and reverse-transcribed into cDNA using a reverse transcription kit. *Lactobacillus* spp. in mouse feces was assessed using qPCR. qPCR was conducted on a LightCycler96 real-time PCR system (Roche, Switzerland). The primer sequences are shown in Table S4.

## Immunofluorescence

Immunofluorescence was performed as previously described. Briefly, KGN cells were fixed with 4% paraformaldehyde and permeabilized with 0.1% Triton X-100. Anti-SOX7 primary antibody was conducted overnight at 4°C and secondary antibody for 60 min at room temperature.

Confocal immunofluorescence microscopy (Zeiss, Oberkochen, Germany) was performed on KGN cells.

## Western blot

The total protein isolated from cells and the protein concentration was measured using the BCA protein assay kit, and lysates were mixed with 5 $\times$  SDS loading buffer in a ratio of 1:4 and then denatured at 98°C for 10 min. Thirty micrograms of each sample were separated on 10% SDS-polyacrylamide gels and then transferred onto PVDF membranes. After blocking with 5% skim milk, the blots were incubated with primary antibodies at 4°C overnight and secondary antibodies for 1 h at room temperature. The membranes were exposed to an ECL western blotting substrate. Signals were recorded using a Syngene bioimaging system (Gene Gnome, Hong Kong, China). The images in the figures represent five individuals. The image acquisition and densitometric analysis of the gel were performed using ImageJ software (<https://imagej.nih.gov/ij>). Primary and secondary antibodies for western blotting were as follows: Anti-SOX7; anti-BAX; Anti-BCL2; anti-GAPDH; HRP-conjugated anti-rabbit; and donkey anti-goat.

## Nuclear and cytoplasmic separation

Nuclear and cytoplasmic assays were conducted using a Nuclear and Cytoplasmic Extraction Kit according to the manufacturer's instructions. Briefly,  $1 \times 10^8$  cells were centrifuged at 1000  $\times$ g for 3 min and resuspended in 500  $\mu$ L of ribonuclease inhibitor added in Nc-Buffer A. Thereafter, Nc-Buffer B was added and incubated on ice for 10 min. The mixtures were then centrifuged at 12,000  $\times$ g at 4°C for 15 min. The supernatants (cytoplasm) were harvested, and the nuclear pellets were resuspended in 250  $\mu$ L of ribonuclease inhibitor in Nc buffer. The mixtures were incubated on ice for 30 min, vortexed every 10 min, and then centrifuged at 12,000  $\times$ g at 4°C for 15 min. The supernatants (nucleus) were then harvested.

## ChIP-seq analysis

KGN cells were seeded at a density of  $2 \times 10^8$  cells per dish and treated with or without cisplatin. Cells were then cross-linked with formaldehyde for 10 min. Chromatin isolation and sonication were performed as described previously.<sup>64</sup> Immunoprecipitation (IP) was performed with an antibody against Sox7 using a Simple ChIP Plus Enzymatic Chromatin IP Kit, according to the manufacturer's instructions. Library preparation and quantification were performed by Novogene (Beijing, China). Library quality was assessed using the Agilent Bioanalyzer 2100 system. Raw data (raw reads) in fastq format were first processed using fastp software.<sup>65</sup> The reference genome and gene model annotation files were downloaded directly from the genome website. The index of the reference genome was built using BWA (v 0.7.12), and clean reads were aligned to the reference genome using BWA mem (v 0.7.12). For a specific ChIP-Seq binding site, individual reads, mapped to the plus or minus strand, presented significant enrichment. For single-end sequencing, the fragment size was estimated using the MACS2 prediction method with default parameters. After mapping reads to the reference genome, we used MACS2 (version 2.1.0) peak-calling software to identify regions of IP enrichment in the background. A q-value threshold of 0.05 was used for all datasets. After peak calling, the distribution of chromosome distribution, peak width, fold enrichment, significance level, and peak summit number per peak were displayed. Samples were input-subtracted, and the data of the precipitated DNA was visualized using an integrated genome viewer, <http://broadinstitute.org/igv>.

### Dual-luciferase reporter gene system

A dual-luciferase reporter assay was performed in KGN cells. Briefly, the pGL3-Bax promoter, pUC-Sox7, and pRL-TK plasmids (Genemei Biotech, Guangzhou, China) were co-transfected with Lipofectamine 3000 reagent. The pUC-basic and pUC-empty vectors were used as controls. After transfection for 48 h, luciferase activity was quantified using a commercial kit (Promega, WI, USA) according to the manufacturer's instructions.

### QUANTIFICATION AND STATISTICAL ANALYSIS

The data in this study are presented as mean  $\pm$  standard error of the mean (SEM), and statistical analyses were performed using GraphPad Prism (version 7.0). According to different types of data, statistical analysis between two groups was performed using the Wilcoxon rank-sum test or Student's *t* test, and one-way analysis of variance (ANOVA) or Dunnett's test was used for multi-group comparisons. Correlation analyses were performed using Spearman's rho statistics. Multiple hypotheses were adjusted using the Benjamini and Hochberg method.<sup>66</sup> In the figures,  $p < 0.05$  indicates statistical significance (\* $p < 0.05$ , \*\* $p < 0.01$ , \*\*\* $p < 0.001$ ). Statistical analyses and data visualization were performed using R V.3.5.0 (RStudio V.1.1.453).